Butyrolactol A is a phospholipid flippase inhibitor that potentiates the bioactivity of caspofungin against resistant fungi

Xuefei Chen,[1, 7] H. Diessel Duan,[2, 7] Michael J. Hoy,[3] Kalinka Koteva,[1] Michaela Spitzer,[1] Allison K. Guitor,[1] Emily Puumala,[4] Guanggan Hu,[5] Bonnie Yiu,[4] Sommer Chou,[1] Zhuyun Bian,[3] Amelia Bing Ya Guo,[1] Sheng Sun,[3] Nicole Robbins,[4] Michael A. Cook,[1] Ray Truant,[6] Lesley T. MacNeil,[1,6] Eric D. Brown,[1] James W. Kronstad,[5] Leah E. Cowen,[4] Joseph Heitman,[3] Huilin Li,[2, *] and Gerard D. Wright[1, 8, *]

[1]David Braley Centre for Antibiotics Discovery, M.G. DeGroote Institute for Infectious Disease Research, Department of Biochemistry and Biomedical Sciences, McMaster University, Hamilton, Ontario, L8S 4K1, Canada

[2]Department of Structural Biology, Van Andel Institute, Grand Rapids, MI 49503, USA

[3]Department of Molecular Genetics and Microbiology, Duke University, Duke University Medical Center, Durham, NC 27710, USA.

[4]Department of Molecular Genetics, University of Toronto, Toronto, Ontario, M5G 1M1, Canada.

[5]Michael Smith Laboratories, Department of Microbiology and Immunology, University of British Columbia, Vancouver, BC, Canada

[6]Department of Biochemistry and Biomedical Sciences, McMaster University, Hamilton, ON L8S 4L8, Canada

[7]These authors contributed equally

[8]Lead contact

[*]Correspondence: huilin.li@vai.org (H.L.); wrightge@mcmaster.ca (G.D.W.)

Summary

Fungal infections cause millions of deaths annually and are challenging to treat due to limited antifungal options and increasing drug resistance. Cryptococci are intrinsically resistant to the latest generation of antifungals, echinocandins, while *Candida auris*, a notorious global threat, is also increasingly resistant. We performed a natural product extract screen for rescue of the activity of the echinocandin caspofungin against *Cryptococcus neoformans* H99, identifying butyrolactol A, which restores echinocandin efficacy against resistant fungal pathogens, including *C. auris*. Mode of action studies revealed that butyrolactol A inhibits the phospholipid

flippase Apt1–Cdc50, blocking phospholipid transport. Cryoelectron-microscopy analysis of the Apt1●butyrolactol A complex revealed that the flippase is locked in a dead-end state. Apt1 inhibition disrupts membrane asymmetry, vesicular trafficking, and cytoskeletal organization, thereby enhancing echinocandin uptake and potency. This study identifies flippases as promising antifungal targets and demonstrates the potential of revisiting natural products to expand the antifungal arsenal and combat resistance.

Keywords

Cryptococcus, *Candida auris*, antifungal, natural product, fungal resistance, flippase, butyrolactol A, synergy, caspofungin

Introduction

More than a billion people suffer from disseminated fungal infections worldwide, and fungi are responsible for >2.5 million human deaths annually,[1, 2] exceeding tuberculosis and malaria.[3, 4] The World Health Organization and Centers for Disease Control and Prevention have raised the alarm that strains of multidrug-resistant *Candida auris*, for example, are a growing global threat.[5] Furthermore, members of the genus *Cryptococcus* are among the most critical fungal challenges, causing meningitis, pneumonia, and central nervous system disease.[6, 7] Cryptococcal meningitis is the most prevalent disseminated fungal disease in AIDS patients, responsible for 15% of AIDS-related deaths annually (>181,000), with mortality rates approaching 100% if infections remain untreated.[8, 9]

Despite the impact of fungal infections on human health, treatment options are limited to only three major drug classes approved for clinical use.[8, 10] Polyenes such as amphotericin B (AMB), which binds the fungal membrane sterol ergosterol, remain a primary treatment option for cryptococcosis despite severe side effects such as hemolysis.[11] Azole antifungals are another commonly used drug class that targets ergosterol biosynthesis but generally exerts fungistatic effects, increasing the risk of developing resistance.[12, 13] Though the pyrimidine antimetabolite 5-fluorocytosine can be effectively paired with azoles or AMB, it is not used as a monotherapy because of the rapid emergence of resistance and is not approved or available in much of the developing world.[14, 15] The latest class of antifungal drugs, the echinocandins, are ineffective against cryptococci, and resistant C. *auris* strains are increasingly common.

Echinocandins, such as the semi-synthetic drug caspofungin (Figure 1A), inhibit the β-(l,3)-D-glucan synthase Fks1 subunit, which is responsible for polymerizing the essential polysaccharide component of most fungal cell walls, resulting in fungal cell lysis.[16, 17] The absence of cell walls in mammalian cells has made echinocandins highly successful, low-toxicity antifungal drugs.[18, 19] The gene encoding β-(l,3)-D-glucan synthase Fks1 subunit is essential for *C. neoformans* viability, and the purified cryptococcal β-(l,3)-D-glucan synthase is inhibited by echinocandin drugs *in vitro*.[20, 21] Nevertheless, cryptococci are intrinsically resistant to echinocandin therapy in part due to the action of cell division control protein 50 (CDC50), the noncatalytic subunit of a binary lipid flippase complex.[22, 23] An antifungal peptide targeting the extracellular loop of Cdc50 enhances caspofungin activity with a fractional inhibitory concentration index (FICI) of 0.5, demonstrating a promising strategy to sensitize *Cryptococcus* to caspofungin via CDC50 inhibition, despite the modest synergy.[24]

Identifying adjuvants that inhibit antifungal resistance offers a means to repurpose echinocandins as anti-cryptococcal drugs and to rescue their activity against other resistant organisms.[25] Reasoning that natural products offer an untapped source of echinocandin potentiators, we screened a subset of our collection of microbial extracts[26] for compounds that sensitize *C. neoformans* to caspofungin. We report the discovery of butyrolactol A, a polyketide antifungal natural product that we demonstrate unexpectedly enhances echinocandin activity against cryptococci and drug-resistant *Candida* spp. by inhibiting the Apt1–Cdc50 phospholipid flippase. This mode of action enriches our limited antifungal arsenal and offers an orthogonal combination strategy to combat drug-resistant fungal infections.

Results

A high throughput screen for potentiators of caspofungin against *C. neoformans* H99 identifies butyrolactol A

Approximately 4,000 methanolic extracts derived from our in-house collection of actinomycetes and fungi[26] were screened against *C. neoformans* H99 in the presence and absence of 4 µg/mL caspofungin (1/8 MIC) (Figure 1A, S1A). Six extracts exhibited effective and reproducible caspofungin potentiating capacity against *C. neoformans* in a dose-dependent manner (Figure S1B). The anticancer compound actinomycin D, associated with significant human cell toxicity, was identified from WAC237 and WAC1315 as a caspofungin adjuvant (Figure S1C-S1D). The

remaining four isolates, WAC205, WAC6266, WAC6818, and WAC8370 produced the same caspofungin potentiator, compound **1** (Figure S1E). Structural elucidation of compound **1** by high-resolution mass spectrometry (HRMS), coupled with one- and two-dimensional NMR spectroscopy, identified it as butyrolactol A (BLA), an antifungal polyketide polyol first reported in 1992 from *Streptomyces rochei* S785-16 (Figure S1F).[27]

A synthetic biology strategy to develop high-yield producers of butyrolactol A and B

We sequenced the genome of the BLA producer WAC8370, a strain of *Streptomyces ardesiacus*, and identified the predicted BLA biosynthetic gene cluster (BGC) based on the type I polyketide synthase (PKS) previously reported for BLA biosynthesis in the marine-derived *Streptomyces sp*. NBRC 110030 (Figure S2A, Table S1).[28] To facilitate downstream studies, we generated a high-yield heterologous expression producer of BLA through transformation-associated recombination of a 71,401 bp genomic region of WAC8370 in *Streptomyces coelicolor* M1146, a model actinomycete chassis (Figure 1B, S2B).[29] Surprisingly, instead of BLA, the construct yielded a compound with [M-H]□ ions of *m/z* 511.29, 14 *m/z* units less than standard BLA, consistent with the absence of a methyl group (Figure 1C, S2C). Further structural analysis revealed that the compound was butyrolactol B (BLB), which has a terminating isopropyl group instead of the *t*-butyl of BLA (Figure 1C, S2D). Thus, we focused on identifying the missing methyltransferase necessary for BLA biosynthesis.

The *t*-butyl tail is a noteworthy BLA structural feature, which has been found in metabolites of marine cyanobacteria but is rarely seen in actinomycetes.[30] Stable isotope feeding experiments found that the source of the *t*-butyl tail is Val; therefore, synthesis of BLA likely requires a rare C-methylation at the isopropyl secondary carbon.[31] AprA is a unique methyltransferase that acts in the PKS initiation steps for the *t*-butyl starter of the marine-derived natural product apratoxin A.[32] Three potential analogs of AprA were found in the WAC8370 genome, all of whose structures were predicted by AlphaFold 2 and aligned to AprA (Figure S2E-S2G).[33] One candidate is a Class I SAM-dependent methyltransferase located ~2 kb downstream of the BLB BGC, showing 30% identity and 1.562 Å RMSD to AprA (Figure S2A, S2E). This methyltransferase gene was cloned to pIJ10257[34] controlled by the constitutive *ermE** promoter and conjugated into the construct carrying the BLB gene cluster (Figure S2E). The recombinant strain reliably produced BLA at a concentration >10-fold compared to the

natural producer WAC8370 and was sustained over at least seven days of fermentation (Figure 1C, S2H).

Butyrolactol A synergizes with caspofungin in *Cryptococcus spp.* and resistant *Candida auris*

We identified BLA through its ability to potentiate caspofungin against *Cryptococcus* at a single concentration in the initial screen. Thus, we further explored the dose-dependent impact of BLA alone and in combination with caspofungin against *C. neoformans*, *Cryptococcus gatti* - responsible for outbreaks of cryptococcosis on the West Coast of North America in immunocompetent individuals, and caspofungin-resistant *C. auris*, a pathogen of growing concern and associated with several outbreaks.[35, 36]

BLA alone was an effective antifungal with single-digit MICs against various yeast pathogens, including *Cryptococcus* strains, and the filamentous fungi *Aspergillus fumigatus* and *Trichophyton rubrum* (Table S2). Furthermore, BLA demonstrated conserved synergy (Fractional Inhibitory Concentration Index [FICI] ≤ 0.5) with caspofungin across *Cryptococcus* species (Figure 2A).[25] The potentiation at a concentration of half the MIC of BLA significantly decreases the MIC of caspofungin against refractory pathogens to the National Committee for Clinical and Laboratory Standards Institute (CLSI) breakpoint of ≤ 2 μg/mL or below (Table S3). The Rescue Concentration is the concentration of adjuvant that reduces the antimicrobial agent to the breakpoint.[25] BLA is highly effective with a rescue concentration of 0.5-1 μg/mL for caspofungin against *C. neoformans* and *C. gattii* and 2 μg/mL for resistant *C. auris* CBS12766 and CBS12776, despite its modest activity when used alone (Figure 2A, Table S3).

The potentiation profile of BLA was further examined in the *Galleria mellonella* and *Caenorhabditis elegans* animal infection models, which are frequently employed to study Candida-host interactions due to the ease of infection and functional similarity.[37, 38] BLA (0.5 mg/kg; ¼ MIC) and caspofungin (4 mg/kg; ¼ MIC) alone showed no significant *in vivo* activity against *C. neoformans* H99 in the *G. mellonella* infection model at these low concentrations. At the same time, the combination significantly extended the lifespan of infected larvae compared to individual drug treatments (Figure 2B). Similarly, when examining the efficacy of the compounds against *C. auris* in the *C. elegans* infection model, low concentrations of BLA and caspofungin alone (1/16 MIC) had no significant impact on worm survival. However, BLA and

caspofungin in combination significantly increased the survival of *C. elegans* relative to individual treatments (Figure 2B), highlighting the efficacy of the combination against *C. auris in vivo*.

Butyrolactol A perturbs sterol homeostasis but does not target ergosterol or cell wall biosynthesis.

AMB directly binds and extracts ergosterol from lipid bilayers. We observed that the AMB-resistant *C. albicans* ATCC 200955 is also insensitive to BLA, exhibiting an increase in MIC by more than 64-fold compared to reference strains (Table S2). This strain's impaired sterol biosynthesis pathway (Figure 3B-3C)[39] makes it resistant to other ergosterol biosynthesis inhibitors, such as fluconazole and terbinafine (Figure 3A, Table S2). This cross-resistance and related structures (polyketide polyols) between BLA and AMB (Figure 3D) suggested that they might share a similar mechanism of action.[40, 41] If BLA shared the same mechanism as AMB, we reasoned that supplementing cultures with ergosterol would mitigate its toxicity. However, the addition of exogenous ergosterol failed to rescue cell viability during BLA treatment, while it showed a striking and dose-dependent reversal of the fungicidal activity of AMB (Figure 3E), indicating that BLA operates through a mechanism different from AMB.

To assess if BLA affected sterol homeostasis, the amount of ergosterol in membranes following treatment with BLA was measured by GC-MS in both *C. neoformans* and *C. albicans*. Control drugs fluconazole and terbinafine caused a marked decrease in ergosterol upon the interruption of ergosterol (*erg*) biosynthesis genes, *ERG11* and *ERG1*, respectively (Figure 3A, 3F). BLA treatment resulted in a mild reduction of ergosterol in *C. neoformans* H99, and a significant depletion (61%) of ergosterol in *C. albicans* ATCC90028, suggesting the compound affects sterol homeostasis in a manner distinct from AMB (Figure 3F). To further explore the potential impact of BLA on ergosterol biosynthesis, we tested eleven *C. albicans* mutants containing heterozygous gene deletions in the *erg* pathway for hypersensitivity to BLA. No *erg* mutants were sensitized to BLA, suggesting that ergosterol biosynthesis enzymes are not the direct molecular target of BLA (Figure 3G). On the other hand, heterozygous deletion of *erg* genes did confer some resistance to BLA, as evidenced by growth curve analysis of each mutant with and without BLA (1.56 μM), suggesting that membrane composition is vital for the activity

of BLA (Figure 3G and 3H). Additionally, osmotic protection did not affect the fungicidal activity of BLA, while it increased the MIC of caspofungin against *C. albicans* by 64-fold (Table S2), consistent with no impact on the cell wall.

Identification of butyrolactol A as a novel inhibitor of the flippase complex Apt1–Cdc50

While our genetic and phenotypic characterizations suggest that BLA impacts sterol homeostasis, the mechanism(s) by which it does so remained elusive. To elucidate potential targets, we selected for resistant mutants coupled with genome sequencing.[42] Two *C. neoformans* H99 BLA-resistant mutants were generated by three passages in liquid culture at half-MIC, followed by selection on corresponding MIC plates, and final isolation from 4×MIC BLA agar plates (Figure S3A). Genome sequencing identified a common mutated gene, CNAG_06469 (*APT1*), which encodes a P4-ATPase, also known as lipid flippase, belonging to the Drs2-related P4A subfamily (Figure 4A).[43] The mutations in *APT1* included a 22-base tandem duplication insertion in region 557845-557867, causing a frameshift downstream in the C-terminal tail (RA3) and a mutation within the actuator (A) domain at position 561541 (G266V, RA4) (Figure 4A). To determine if these *APT1* mutations are responsible for BLA resistance, a genetic backcross was performed to generate progeny, which was screened for the resistance phenotype and subsequently genotyped. Nearly 1:1 segregation patterns of the resistance phenotype were determined in both RA3 X KN99**a** and RA4 X KN99**a** F1 progeny, suggesting a single genetic locus was responsible for this phenotype (Figure 4B, Table S4). Each progeny was genotyped to reveal that the inherited parental *APT1* allele segregated with the resistance phenotype, demonstrating that the *APT1* mutant variant is responsible for the resistance (Table S4).

Finally, the resistance of a cryptococcal *apt1*Δ mutant to BLA further confirmed that Apt1 is a likely target of BLA and highlighted the mutations identified in the resistant mutants were loss of function (Figure 4C). Most P4-ATPases are binary complexes containing a subunit from the CDC50 family. The only member of this family in *C. neoformans*, Cdc50, was identified as a β-subunit for Apt1, forming a stable complex that functions as a lipid flippase.[44, 45] Therefore, the susceptibility of *cdc50*Δ and *apt1*Δ *cdc50*Δ mutants was characterized. We observed that depletion of CDC50 resulted in severe growth defects in RPMI medium, which mimics *in vivo* physiological conditions, particularly at 37 °C. This finding aligns with previous reports of impaired survival of *cdc50Δ* mutants in mouse models, underscoring the critical role of

CDC50 in the *in vivo* survival of fungal pathogens.[22, 44] In acidic, carbon-enriched SDB medium, commonly used for rapid fungal culture, the *cdc50*Δ and *apt1*Δ *cdc50*Δ mutants displayed similar resistance to BLA as *apt1*Δ, suggesting that BLA targets the flippase complex (Figure 4C). Besides Apt1, three other P4-ATPase genes were identified in the cryptococcal genome (*APT2*, *APT3*, and *APT4*). Only the *apt2*Δ mutant exhibited modest BLA resistance, likely due to its close phylogenetic relationship to Apt1 (Figure 4C, S3B). The enhanced resistance observed in the double mutant *apt1*Δ *apt2*Δ suggests functional redundancy between Apt1 and Apt2 (Figure 4C).

Apt1 and Apt2 are closely related to the plasma membrane P4-ATPases Dnf1/2 from *S. cerevisiae*, which have broad substrate specificity and do not require a phosphate group for lipid substrate recognition (Figure S3B).[46] The transmembrane flippase, often associated with an indispensable β-subunit belonging to the Cdc50 family, drives an inward translocation of various phospholipids to establish an essential asymmetric lipid distribution of the membrane with phosphatidylserine (PS) and phosphatidylethanolamine (PE) concentrated within the cytosolic leaflet.[47, 48] Cdc50 depletion results in a loss of membrane asymmetry that exposes PS on the extracellular leaflet.[22, 44] The inhibitory effect of BLA on the flippase function of Apt1–Cdc50 was validated by monitoring PS accumulation on the extracellular leaflet, which specifically binds to green fluorescent conjugated annexin V.[22] Increasing PS exposure on the extracellular leaflet of the membrane under BLA treatment is consistent with the model where BLA inhibits the flippase complex, blocking phospholipid translocation and resulting in disrupted membrane asymmetry (Figure 4D).

The amphipathic BLA shares structural similarities to the natural substrates of the flippase, specifically a hydrophobic tail and a hydrophilic head that binds to the protein.[46, 49] Thus, we reasoned that given the broad substrate specificity of the Apt1–Cdc50 complex, BLA might be mistakenly loaded as a substrate analog,[45] inhibiting flippase activity in a competitive manner, obstructing the lipid entrance and leading to PS accumulation on the extracellular leaflet.[48] Exogenous PS was supplied as a potential competitor of BLA, which did not affect the growth of cryptococcal cells but effectively restored the severe growth defect in the presence of BLA to the level of untreated/resistant cells (Figure 4E). Furthermore, other phospholipids such as phosphatidylcholine (PC), phosphatidylethanolamine (PE), and the phospholipid precursor

phosphatidic acid (PA) also conferred some rescue of *C. neoformans* growth, while triacylglycerol (TAG), which lacks a hydrophilic head, did not (Figure S3C).

To further explore the proposed mode of action (MOA), the relationship between the flippase complex and the uptake ratio of BLA was investigated.[50] Deletion of *cdc50* significantly reduced BLA uptake, and deletion of *apt1* moderately decreased its uptake, possibly due to the redundant contributions of the flippase catalytic subunits, suggesting an interaction between BLA and the Apt1–Cdc50 complex (Figure 4C and 4F). In contrast, both deletions resulted in increased uptake of AMB, which is consistent with the distinct MOA proposed for the two compounds (Figure S3D).[22, 43] In addition to serving as an integral part of the lipid translocating machinery for P4-ATPases, Cdc50 also functions as a chaperone, facilitating the exit of flippases from the endoplasmic reticulum (ER) to their correct destinations.[51] BLA disrupts the chaperone activity of Cdc50, causing mislocalization of Apt1 as observed with a C-terminal epitope-tagged Apt1-DsRed. Under normal conditions, Apt1-DsRed cycles between the Golgi,[52] endosomes as punctate structures distributed throughout the cell, and the cell membrane.[53, 24] However, BLA treatment leads to its accumulation in the ER and increased retention at the cell membrane (Figure 4G), indicating impaired retrieval and endocytosis pathways due to suppressed Cdc50 and Apt1 activity.[54, 55]

Cryo-EM reveals butyrolactol A binding to Apt1–Cdc50 and obstruction of the lipid transport channel

Cryo-electron microscopy (cryo-EM) studies were conducted to further elucidate the molecular mechanism of BLA-mediated flippase inhibition and its interactions with Apt1–Cdc50. We heterologously co-expressed the full-length *C. neoformans* Apt1 and Cdc50 in *S. cerevisiae* BY4741 *pep4Δ* and purified the heterodimeric protein complex using the detergents lauryl maltose neopentyl glycol (LMNG) and cholesteryl hemisuccinate (CHS). ATP was supplemented during the purification wash steps to remove endogenously bound lipids from lipid-bound flippases.[56]

As a P4-ATPase, Apt1–Cdc50 operates via the Post-Albers mechanism, where cyclic phosphorylation and dephosphorylation in the cytoplasmic ATPase domain drive phospholipid translocation, generating intermediate states with distinct substrate affinities.[57] In the E2P state, a hydrophilic cleft opens toward the extracellular/luminal leaflet, enabling substrate lipid loading

and polar headgroup binding, representing a high-affinity state for transported substrates.[48] Substrate lipids have been captured at the entry sites of their respective E2P-state flippases, serving as lipid cargos poised for translocation.[58, 59, 60, 61] Recognizing that BLA competes with the substrate lipid for the same binding site, we locked Apt1–Cdc50 in the E2P state using the phosphate analog BeF_3^- and resolved the BLA-bound cryo-EM structure at an overall resolution of 2.7 Å (Figure 5A and S4, Table S5). To compare and validate the competition model, the E1 state of the flippase complex was also determined (Figure S5, Table S5).

An elongated EM density was observed within the lipid entry groove, aligning closely with the BLA molecule. The structure is clearly in the expected E2P state, supported by the well-ordered autoregulatory C-tail composed of the GFGFT motif and a short α-helix (Figure 5A).[57, 62] Notably, the BLA binding prominently induced the closure of the lipid entry site (Figure 5A, 5B). The γ-butyrolactone moiety of BLA is stabilized by hydrophobic interactions with I481 from the PISL motif of TM4 (Transmembrane Helix 4) and P127 from TM2 (Figure 5A), while the hydroxylated γ-lactone ring is positioned just over 3.5 Å from the conserved residues Q111, Q476, and N477, with potential water-bridged hydrogen bond interactions. The α-hydroxyl group of the lactone ring forms hydrogen bonds with S482 of the TM4 PISL motif and N1109 of TM6, anchoring the lipid-like BLA headgroup to the substrate access channel (Figure 5A). Additionally, two pairs of hydrophobic residues (I119 and Y1102, L123 and L1106) seal the entry site of the substrate channel, preventing further substrate lipids from entering from the membrane matrix (Figure 5B). This binding mode contrasts with that of *S. cerevisiae* Dnf1 in the same E2P state, where the channel entry remains fully open when bound to a substrate lipid such as PC (Figure 5C). Interestingly, the aliphatic tail of BLA appears to jam the transport channel by adopting a kinked configuration by virtue of its conjugated double bonds. The BLA tail extensively interacts with the so-called 'hydrophobic barrier' residues, including I130, I134, I485, I493, and I1118 (Figure 5A, 5B).[48] Despite the distinct effects of lipid-like BLA and substrate lipid PC on the conformation of the lipid transport channel (Figure 5B, 5C, S6A), the E1 states of Apt1 and Dnf1 are similar as both feature a closed channel that is incompatible with substrate binding at the entry site (Figure 5D, 5E, S6B). Collectively, these findings suggest a BLA inhibition mechanism wherein BLA binding induces closure of the lipid entry site and obstructs the transport channel with its kinked tetraene tail, effectively stalling the flippase in an abnormal E2P-like state.

Mutations of the key residues involved in BLA binding (Figure 5A) were prepared using a TRACE (Transient CRISPR-Cas9 coupled with Electroporation) strategy, which overcomes the challenges of genetic manipulation in *Cryptococcus* spp[63]. This approach resulted in 6% correctly integrated constructs, with an epitope FLAG-tag added to the C-terminus of wild-type and mutant Apt1 simultaneously, as verified by sequencing (Figure S7A). The mutations introduced in *APT1* did not significantly affect the flippase's transcriptional or translational expression levels (Figure S7B-S7C). Subsequent susceptibility tests identified residues P127 and N1109 as crucial for BLA binding, as single mutations at either site significantly increased BLA resistance, mirroring that seen in the *apt1* promoter-disrupted mutant in which binding of BLA to the flippase is presumably abolished (Figure 5F). Both alanine substitutions at the equivalent site in the PS flippase ATP11C (i.e., P94A and N912A) exhibited comparable PS-dependent ATPase activities,[56] indicating that the observed BLA resistance in P127A and N1109A mutants results from a loss of binding for the inhibitor BLA rather than natural substrate lipids like PS (Figure 5A). In contrast, single mutations I481A and S482A within the conserved PISL substrate-binding motif did not confer BLA resistance. Given that the equivalent mutation of I481A in ATP11C (i.e., V357A) reduces PS-dependent ATPase activity by over 80% compared to the wild-type enzyme[56] and the equivalent of S482 in ATP8B1 (i.e., S403) has been implicated in substrate recognition,[58] we propose that I481 and S482 preferentially bind natural substrate lipids such as PS over the inhibitor BLA. This reduced natural cargo binding in these mutants may increase BLA binding, thereby mitigating resistance. Indeed, the S482A substitution increased BLA sensitivity two-fold, supporting the crucial role of S482 in stabilizing natural cargos, thus enhancing the competitive binding advantage of BLA, thereby rendering the mutant more susceptible (Figure 5F). Besides these conserved residues in anchoring the BLA headgroup, the middle “hydrophobic barrier” region extensively interacted with BLA's uniquely folded tetraene tail, a feature rarely seen with natural cargos (Figure 5B, 5C). The quintuple mutant, bearing I130A, I134A, I485A, I493A, and I1118A substitutions within the hydrophobic barrier, showed a 2-fold increase in MIC (Figure 5F), suggesting that the tail typically helps stabilize itself within the transport channel, a function that the mutant residues can no longer effectively perform.

BLA inhibition of Apt1−Cdc50 disrupts membrane architecture and trafficking

BLA traps the Apt1–Cdc50 complex in a dead-end state, preventing the flippase from completing the catalytic cycle. Previous studies have highlighted the overlapping functions of the Apt1 and Cdc50 in maintaining membrane integrity,[44, 45] which may account for the cell death observed following BLA-mediated inhibition. Notably, BLA treatment caused a dose-dependent ATP leakage, with intracellular ATP levels dropping by 13-fold at 3 μM BLA and 38-fold at 6 μM BLA, respectively, alongside a corresponding rise in extracellular ATP (Figure 6A). Membrane disruption became evident within half an hour and intensified over time, leading to a significant increase in ATP leakage (Figure 6B). These findings suggest that the binding of BLA and flippase complex compromises membrane integrity, leading to substantial leakage of cellular contents and ultimately leading to cell death (Figure S8A). The activity of BLA relies on effective binding to the functional Apt1-Cdc50 complex, as mutations in Apt1 or the deletion of either component confer resistance to BLA. Conversely, galactose-induced overexpression of the Apt1–Cdc50 in *S. cerevisiae* resulted in pronounced hypersensitivity to BLA, suggesting that the BLA and Apt1–Cdc50 interaction is toxic to the cell (Figure S8B). This mechanism resembles that of the topoisomerase I (TOP1) inhibitor camptothecin, which does not directly damage DNA but rather traps TOP1 conformation in cleave complexes that interfere with DNA replication and transcription, resulting in cytotoxicity.

Transmission electron microscopy (TEM) provided direct visual evidence of membrane disruption. Untreated cells displayed a typical ultrastructural aspect of cryptococcal morphology (Figure 6C, a), while treatment with 1 μM BLA resulted in significant membrane detachment from the cell wall, indicative of impaired membrane architecture (Figure 6C, b-d). Additionally, abnormal cytoplasmic vacuoles containing lipid bodies were observed, along with large vacuole-like structures over 1 μm in diameter containing fragmented endomembrane pieces (Figure 6C, b-d). These structures resembled the giant vacuoles seen in *apt1*Δ mutants, resulting from the disrupted vacuolar organization.[64] To investigate the disruption process, the BLA concentration was reduced to 0.5 μM, revealing extensive distorted membranous structures, including electron-dense, stacked membranes (green arrowhead) and vesicles (black arrowhead), enlarged atypical vacuoles (AV), mitochondrial swelling, and Berkeley body-like double-membrane compartments (~200 nm), which are widely seen in secretory impaired mutants such as *sec7*, *sec14*, and *drs2* (Figure 6C, e-f).[65, 66] BLA's inhibition of the exocytosis pathway was further confirmed in conditionally-repressible *C. albicans* GRACE mutants.[67] Transcriptional repression of clathrin

heavy chain gene (*CHC1*), *CDC50*, and *PAN1* conferred hypersensitivity to BLA, while overexpression of the transcripts resulted in resistance in *C. albicans* (Figure 6D).[52, 68] Pan1, a homologue of Esp15, localizes to clathrin-coated pits and functions in the same or parallel pathway as Chc1 and Cdc50 for clathrin-coated vesicle formation, suggesting that BLA inhibits the clathrin-dependent secretory pathway.[65, 69]

Given the critical roles of membrane organization in trafficking, the BLA effect on endocytosis was further investigated by assessing the uptake of lipophilic styryl dye FM4-64, which intercalates into the plasma membrane and is internalized via the endocytic pathway, labelling endosomes, vacuoles, and vesicle cycling, as observed in untreated *C. neoformans* cells (Figure 6E).[70] Intensely fluorescent large formations accumulated in BLA-treated cells along with persistent signal retained on the cell membrane, indicating that BLA blocks endocytosis and phospholipid cycling (Figure 6E).[65] Additionally, BLA induced significant morphological changes, suggesting disruption of the actin cytoskeleton. The high-affinity F-actin probe, phalloidin, conjugated to Alexa Fluor 568 dye, was applied, which revealed an aberrant actin distribution in *C. neoformans* cells treated with a low concentration of BLA. Unpolarized actin clumps (~0.8 µm diameter) were observed in ~32% of treated cells, a phenotype typically associated with yeast mutants lacking actin-regulating kinase activity, likely due to unregulated actin nucleation complex Arp2/3 (Figure 6F, Figure S8C).[71] This suggests that BLA impaired actin motility and polarization likely through interaction with Apt1, which is functionally linked to Drs2 and involved in actin polarization and endocytosis.[43, 72] In addition, heterozygous deletion of the actin assembly genes *ARP2*, *ARP3*, *CCT5*, or *CCT6* conferred strong resistance to BLA in *C. albicans* (Figure 6G), further indicating BLA tends to impair actin- and clathrin-mediated endocytosis while sparing the alternative Arp2/3-independent endocytic pathway (AIE).[73]

In addition to influencing actin cytoskeletal organization, membrane lipid composition is essential for determining sensitivity to drugs targeting ergosterol biosynthesis,[72] such that flippase-deficient mutants *Δcdc50* and *Δapt1* exhibited increased susceptibility to fluconazole (Figure S8D).[22, 43] The combination of BLA with amphotericin B, fluconazole, or terbinafine was investigated, revealing a significant synergistic interaction between these agents (Figure 6H). Though P4 ATPases are widely found in eukaryotic cells and are essential for cell membrane homeostasis, BLA showed much lower cytotoxic and hemolytic toxicity than amphotericin B

(Figure S8E, Table S2). The high selectivity of BLA may be attributed to the redundant roles of flippases in mammals (Figure S3B).

Butyrolactol A potentiates the fungicidal activity of caspofungin against *C. neoformans* by inhibiting the Apt1–Cdc50 complex

We propose a model in which BLA competitively inhibits the Apt1–Cdc50 complex, disrupting membrane lipid asymmetry and consequently leading to impaired membrane architecture and the blockage of clathrin-dependent membrane trafficking (Figure 7A). A recent study revealed that Cdc50 is essential for the innate echinocandin resistance of *Cryptococcus* spp. by preventing the uptake of the drug and maintaining intracellular calcium homeostasis that regulates cell wall synthesis and stress responses.[22, 23] Both *cdc50*Δ and *apt1*Δ *cdc50*Δ mutants exhibited hypersensitivity to the calcineurin inhibitor FK506, highlighting the critical role of flippase in calcium regulation (Figure 7B). The equivalent sensitivity observed in *apt1*Δ mutants further suggests that Apt1 and Cdc50 function together to regulate calcium/calcineurin signalling (Figure 7B).

Moreover, deletion of *CDC50* and *APT1* resulted in increased susceptibility to caspofungin, along with significantly elevated caspofungin internalization, demonstrating that both Cdc50 and Apt1 influence caspofungin uptake and potency in *C. neoformans* (Figure 7C-7D). However, the effect of *CDC50* was more pronounced than that of *APT1*, suggesting a broader role for *CDC50* beyond acting as a subunit of *APT1*. Similarly, BLA treatment overcame the limitation of caspofungin uptake, indicating that it potentiates caspofungin activity by inhibiting the Apt1–Cdc50 complex (Figure 7D). This mechanism was further evaluated by examining the interaction in deletion mutants, where the synergistic effect was completely lost in *apt1*Δ, *cdc50*Δ, and *apt1*Δ *cdc50*Δ mutants, confirming that BLA's adjuvant mechanism involves the inhibition of the Apt1–Cdc50 complex (Figure 7E).

Discussion

A significant challenge in developing antifungal agents is that fungi and their hosts share similar eukaryotic cellular machinery and biochemistry. Echinocandins are non-toxic antifungal drugs targeting a unique fungal enzyme, but their impact is eroded by intrinsic and acquired resistance. To rescue echinocandin activity, we developed a cell-based screening approach using our natural

product library to identify adjuvants that restore caspofungin's anti-cryptococcal activity, identifying BLA, a previously reported but understudied antifungal compound of unknown mechanism. BLA overcomes intrinsic caspofungin resistance in cryptococci and resistant *C. auris*, as well as showing good activity on its own against a broad spectrum of pathogenic fungi.

BLA's novel mechanism of action identifies P4-ATPases as promising antifungal targets, offering a strategy to expand the limited antifungal arsenal against drug-resistant pathogens. Flippases mediate phospholipid transport between bilayer leaflets, which is crucial for membrane asymmetry[74] and trafficking[75], vesicle budding,[76] polarity maintenance,[77] and cytoskeletal dynamics.[78] Among the four flippases in *C. neoformans*, Apt1 plays a broader role in survival and virulence,[43, 44, 64, 79] exhibiting features of different subfamilies of P4-ATPases, Drs2 and Dnf1 (Figure 4G).[45, 54] Although Apt1 is evolutionarily closer to Dnf1 (Figure S3B), it functionally resembles Drs2,[45, 54] possessing conserved residues for PS specificity, including Q111 in the QQ motif for PS recognition and N477 for PS headgroup stabilization (Figure S9).[49, 57] The Apt1–Cdc50 complex exhibits broad substrate specificity beyond PS (Figure S3C), allowing for BLA misloading but not TAG, indicating that a hydrophilic headgroup is essential for transport despite the tolerance to structural variations, enlightening the optimization of structural derivatives for enhanced potency.

BLA's killing mechanism requires functional Apt1–Cdc50 to form a toxic complex, disrupting membrane asymmetry, architecture, vesicle trafficking, and cytoskeletal organization, ultimately causing cell lysis and death. This mechanism parallels well-known cases where active protein-ligand complexes lead to drug action, while loss-of-function mutations in target proteins confer resistance. For instance, the topoisomerase I (TOP1) inhibitor camptothecin induces cytotoxicity by trapping TOP1 conformation in cleave complexes, thereby interfering with DNA replication and transcription.[80] Similarly, calcineurin, a Ca^{2+}/calmodulin-dependent phosphatase, is targeted by immunophilin-immunosuppressant complexes, such as cyclophilin A-cyclosporin A (CyPA-CsA) and FKBP12-FK506. Mutations in CyPA or FKBP12 confer resistance to CsA and FK506, respectively.[81, 82] In addition, rapamycin also targets FKBP12 but forms distinct protein-ligand complexes that disrupt different signaling pathways, leading to immunosuppression through a distinct mechanism.[83, 84] These examples underscore the importance of protein-ligand complexes as the active entities, rather than the small ligands alone.

Although Apt1 and Cdc50 form a stable complex that supports flippase activity and share several phenotypic similarities in gene-depleted mutants, a significant growth defect was only observed in *cdc50Δ* mutants.[44, 45] Nonetheless, spontaneous mutations were found exclusively in *apt1* across independent resistant mutants, suggesting that *cdc50* mutations conferring BLA resistance likely incur a substantial fitness cost. As the sole member of the CDC50 family in *Cryptococcus*, Cdc50 may have broader roles beyond chaperoning, such as regulating salt stress, acidic pH, iron metabolism, membrane integrity, and cytoplasmic calcium homeostasis.[23, 44] The role of Cdc50 in the physiology and pathogenesis of *C. neoformans* warrants further investigation. Recent research indicates that Cdc50 is essential for cryptococcal resistance, although the underlying mechanisms remain unclear.[22, 85] A synthetic peptide designed to block Cdc50 has shown promise in sensitizing *Cryptococcus* to caspofungin, despite a relatively high FICI, highlighting the potential for rational drug design targeting Cdc50.[24] Our high-resolution structure of the Apt1–Cdc50–BLA complex provides new opportunities for designing inhibitors that mimic native substrates and effectively target both subunits of the flippase complex.

RESOURCE AVAILABILITY

Lead contact

Further information and requests for resources should be directed to and will be fulfilled upon reasonable request by the lead contact, Gerard D. Wright (wrightge@mcmaster.ca).

Materials availability

Strains and plasmids generated in this study are available upon request to the lead contact.

Data and code availability

The Whole Genome Shotgun project of *Streptomyces* sp. WAC8370 has been deposited in GenBank under accession number JBIEOC000000000. The version described in this paper, JBIEOC010000000 (BioProject accession PRJNA1166230), is publicly available as of the publication date.
The experimental NMR data have been deposited in Mendeley Data (DOI: 10.17632/k67455yvv3.1) and are accessible as of the publication date.

The cryo-EM 3D maps of the *C. neoformans* E2P state of Apt1–Cdc50 with bound butyrolactol A and the E1 state of Apt1–Cdc50 have been deposited in the Electron Microscopy Data Bank under accession codes EMD-47338 and EMD-47339, respectively. The consensus refined EM map of the E2P state of Apt1–Cdc50 with bound butyrolactol A is under accession code EMD-47334. The focused refined map of butyrolactol A binding site has accession code of EMD-47335. The atomic models of the E2P state of Apt1–Cdc50 with bound butyrolactol A and the E1 state of Apt1–Cdc50 have been deposited in the Protein Data Bank under accession codes 9DZU and 9DZV, respectively.

Any additional information required to reanalyze the data reported in this paper is available from the lead contact upon request.

ACKNOWLEDGMENTS

This work was supported by the Canadian Institutes for Health Research [project grant PJT190298 to G.D.W.] and the U.S. National Institutes of Health grant R01CA231466 (to H.L.) and the Van Andel Institute (to H.L.).

Studies in the Heitman lab (MH, ZB, SS, and JH) were supported by NIH/NIAID R01 grants AI39115-27, AI050113-20, AI170543-02, AI172451-02, and AI133654-07, and NIH predoctoral fellowship F31 AI150120. J.K. and G.W. are fellows and L.C. and J.H. are fellows and co-directors for the CIFAR program Fungal Kingdom: Threats & Opportunities. J.K. is supported by NIH/NIAID R01 grant AI053721-20.

L.E.C. is supported by the Canadian Institutes of Health Research (CIHR) Foundation grant (FDN-154288) and a National Institutes of Health (NIH) R01 grant (R01AI127375). L.E.C. is a Canada Research Chair (Tier 1) in Microbial Genomics & Infectious Disease and co-Director of the CIFAR Fungal Kingdom: Threats & Opportunities program. CIFAR Catalyst Grants on BLA: CP21-065; Cowen, L. (University of Toronto); Heitman, J. (Duke University); Wright, G. (McMaster University); and Boone, C (University of Toronto).

This research was supported by a Tier 1 Canada Research Chair award and a Foundation grant from the Canadian Institutes of Health Research (CIHR; FRN 143215) to E.D.B.; CIHR funding MOP-119391 to R.T.; and a CIHR grant PJT-156067 to L.M.

The authors wish to express their gratitude to the Centre for Microbial Chemical Biology (CMCB), particularly Tracey Campbell, Susan McCusker, and Nicola Henriquez, as well as the Canadian Centre for Electron Microscopy (CCEM), with special thanks to Marcia Reid, and the McMaster Centre for Advanced Light Microscopy (CALM), with appreciation for the support of Mouhanad Babi. Cryo-EM images were collected in the David Van Andel Advanced Cryo-Electron Microscopy Suite at Van Andel Institute. We thank Dr. Gongpu Zhao and Dr. Xing Meng for facilitating data collection. We are deeply grateful to Dr. Seok-Yong Lee, Dr. Jiyong Hong, Dr. Kenichi Yokoyama, Dr. Marco Dias Coelho, Dr. Vikas Yadav, Dr. Jun Huang, Ziyan Xu, and Anna Floyd Averette for their valuable expertise, guidance, and support during X.C.'s time at the Heitman Lab, Duke University. Acknowledgments are also due to Dirk Hackenberger (McMaster University) for his assistance with bioinformatics analysis. Finally, we thank Linda Ejim, Dr. David Sychantha, Dr. Nicholas Waglechner, Dr. Grace Yim, Dr. Shawn French, Dr. Matt Surette, Dr. Elizabeth Culp and Dr. Haley Zubyk for their valuable support and insightful suggestions.

AUTHOR CONTRIBUTIONS

X.C. and G.D.W. led the project, designed experiments, interpreted data, and wrote the manuscript, with input from all authors. X.C., M.S. and G.D.W. conceived the study. H.D.D. and H.L. designed the cryo-EM study, with X.C. purifying the compound and generating the Apt1–Cdc50 overexpression construct. H.D.D. purified the protein complex, conducted cryo-EM, and built atomic models. M.H. and X.C. designed and conducted the BLA-resistant mutant generation study. M.H. and S.S. performed the genetic cross-assay and analyzed the data, with S.S. generating the double deletion mutants. X.C. prepared the genomic DNA, and A.G. performed genome sequencing and data analysis. M.S. designed, conducted and analyzed the screen, and M.A.C. performed additional statistical analysis. K.K., M.S. and X.C. performed structural elucidation. E.P., B.Y., and N.R. performed dose-response assays on *C. albicans* mutants. S.C. and X.C. conducted the *C. elegans* animal study. G.H. constructed the DsRed-Apt1p. X.C. and Z.B. generated single-point mutations in cryptococcal *APT1*. R.T., A.B.Y.G. and X.C. performed wide-field microscopy. X.C. designed and performed all other experiments. R.T., L.M., E.D.B., J.K., L.C., J.H., H.L., and G.D.W. provided resources.

DECLARATION OF INTERESTS

L.E.C. is a co-founder and shareholder in Bright Angel Therapeutics, a platform company for the development of novel antifungal therapeutics. E.D.B is the CEO and L.E.C. and G.D.W. are Science Advisors for Kapoose Creek, a company that harnesses the therapeutic potential of fungi. All other authors have no competing interests to declare.

SUPPLEMENTAL INFORMATION

Figures S1–S9 and Table S1–S5

Reference

1. Iliev, I.D., Brown, G.D., Bacher, P., Gaffen, S.L., Heitman, J., Klein, B.S., and Lionakis, M.S. (2024). Focus on fungi. Cell *187*, 5121–5127. https://doi.org/10.1016/j.cell.2024.08.016.

2. Denning, D.W. (2024). Global incidence and mortality of severe fungal disease. Lancet Infect. Dis. *24*, e428–e438. https://doi.org/10.1016/S1473-3099(23)00692-8.

3. Brown, G.D., Denning, D.W., Gow, N.A.R., Levitz, S.M., Netea, M.G., and White, T.C. (2012). Hidden Killers: Human Fungal Infections. Sci. Transl. Med. *4*, 165rv13-165rv13. https://doi.org/10.1126/scitranslmed.3004404.

4. Bongomin, F., Gago, S., Oladele, R., and Denning, D. (2017). Global and Multi-National Prevalence of Fungal Diseases—Estimate Precision. J. Fungi *3*, 57. https://doi.org/10.3390/jof3040057.

5. Lionakis, M.S., and Chowdhary, A. (2024). Candida auris Infections. N. Engl. J. Med. *391*, 1924–1935. https://doi.org/10.1056/NEJMra2402635.

6. Maziarz, E.K., and Perfect, J.R. (2016). Cryptococcosis. Infect. Dis. Clin. North Am. *30*, 179–206. https://doi.org/10.1016/j.idc.2015.10.006.

7. WHO fungal priority pathogens list to guide research, development and public health action https://www.who.int/publications/i/item/9789240060241.

8. Iyer, K., Revie, N.M., Fu, C., Robbins, N., and Cowen, L. (2021). Treatment strategies for cryptococcal infection: challenges, advances and future outlook. Nat. Rev. Microbiol. https://doi.org/10.1038/s41579-021-00511-0.

9. Rajasingham, R., Smith, R.M., Park, B.J., Jarvis, J.N., Govender, N.P., Chiller, T.M., Denning, D.W., Loyse, A., and Boulware, D.R. (2017). Global burden of disease of HIV-associated cryptococcal meningitis: an updated analysis. Lancet Infect. Dis. *17*, 873–881. https://doi.org/10.1016/S1473-3099(17)30243-8.

10. Stott, K.E., Loyse, A., Jarvis, J.N., Alufandika, M., Harrison, T.S., Mwandumba, H.C., Day, J.N., Lalloo, D.G., Bicanic, T., Perfect, J.R., et al. (2021). Cryptococcal meningoencephalitis: time for action. Lancet Infect. Dis. *21*, e259–e271. https://doi.org/10.1016/S1473-3099(20)30771-4.

11. Gray, K.C., Palacios, D.S., Dailey, I., Endo, M.M., Uno, B.E., Wilcock, B.C., and Burke, M.D. (2012). Amphotericin primarily kills yeast by simply binding ergosterol. Proc. Natl. Acad. Sci. *109*, 2234–2239. https://doi.org/10.1073/pnas.1117280109.

12. Dunkel, N., Liu, T.T., Barker, K.S., Homayouni, R., Morschhäuser, J., and Rogers, P.D. (2008). A Gain-of-Function Mutation in the Transcription Factor Upc2p Causes Upregulation of Ergosterol Biosynthesis Genes and Increased Fluconazole Resistance in a Clinical *Candida albicans* Isolate. Eukaryot. Cell *7*, 1180–1190. https://doi.org/10.1128/EC.00103-08.

13. Yang, H., Tong, J., Lee, C.W., Ha, S., Eom, S.H., and Im, Y.J. (2015). Structural mechanism of ergosterol regulation by fungal sterol transcription factor Upc2. Nat. Commun. *6*, 6129. https://doi.org/10.1038/ncomms7129.

14. Billmyre, R.B., Applen Clancey, S., Li, L.X., Doering, T.L., and Heitman, J. (2020). 5-fluorocytosine resistance is associated with hypermutation and alterations in capsule biosynthesis in Cryptococcus. Nat. Commun. *11*, 127. https://doi.org/10.1038/s41467-019-13890-z.

15. Loyse, A., Dromer, F., Day, J., Lortholary, O., and Harrison, T.S. (2013). Flucytosine and cryptococcosis: time to urgently address the worldwide accessibility of a 50-year-old antifungal. J. Antimicrob. Chemother. *68*, 2435–2444. https://doi.org/10.1093/jac/dkt221.

16. Sucher, A.J., Chahine, E.B., and Balcer, H.E. (2009). Echinocandins: The Newest Class of Antifungals. Ann. Pharmacother. *43*, 1647–1657. https://doi.org/10.1345/aph.1M237.

17. Groll, A.H., and Walsh, T.J. (2001). Caspofungin: pharmacology, safety and therapeutic potential in superficial and invasive fungal infections. Expert Opin. Investig. Drugs *10*, 1545–1558. https://doi.org/10.1517/13543784.10.8.1545.

18. Denning, D.W. (2002). Echinocandins: a new class of antifungal. J. Antimicrob. Chemother. *49*, 889–891. https://doi.org/10.1093/jac/dkf045.

19. Wall, G., and Lopez-Ribot, J.L. (2020). Current Antimycotics, New Prospects, and Future Approaches to Antifungal Therapy. Antibiotics *9*, 445. https://doi.org/10.3390/antibiotics9080445.

20. Cryptococcus neoformans Resistance to Echinocandins: (1,3)β-Glucan Synthase Activity Is Sensitive to Echinocandins | Antimicrobial Agents and Chemotherapy https://journals.asm.org/doi/10.1128/aac.49.7.2851-2856.2005.

21. Thompson, J.R., Douglas, C.M., Li, W., Jue, C.K., Pramanik, B., Yuan, X., Rude, T.H., Toffaletti, D.L., Perfect, J.R., and Kurtz, M. (1999). A Glucan Synthase *FKS1* Homolog in *Cryptococcus neoformans* Is Single Copy and Encodes an Essential Function. J. Bacteriol. *181*, 444–453. https://doi.org/10.1128/JB.181.2.444-453.1999.

22. Huang, W., Liao, G., Baker, G.M., Wang, Y., Lau, R., Paderu, P., Perlin, D.S., and Xue, C. (2016). Lipid Flippase Subunit Cdc50 Mediates Drug Resistance and Virulence in Cryptococcus neoformans. mBio *7*, e00478-16. https://doi.org/10.1128/mBio.00478-16.

23. Cao, C., Wang, Y., Husain, S., Soteropoulos, P., and Xue, C. (2019). A Mechanosensitive Channel Governs Lipid Flippase-Mediated Echinocandin Resistance in Cryptococcus neoformans. mBio *10*, e01952-19. https://doi.org/10.1128/mBio.01952-19.

24. Tancer, R.J., Wang, Y., Pawar, S., Xue, C., and Wiedman, G.R. (2022). Development of Antifungal Peptides against Cryptococcus neoformans; Leveraging Knowledge about the *cdc50Δ* Mutant Susceptibility for Lead Compound Development. Microbiol. Spectr. *10*, e00439-22. https://doi.org/10.1128/spectrum.00439-22.

25. Wright, G.D. (2016). Antibiotic Adjuvants: Rescuing Antibiotics from Resistance. Trends Microbiol. *24*, 862–871. https://doi.org/10.1016/j.tim.2016.06.009.

26. Cook, M.A., Pallant, D., Ejim, L., Sutherland, A.D., Wang, X., Johnson, J.W., McCusker, S., Chen, X., George, M., Chou, S., et al. (2023). Lessons from assembling a microbial natural product and pre-fractionated extract library in an academic laboratory. J. Ind. Microbiol. Biotechnol. *50*, kuad042. https://doi.org/10.1093/jimb/kuad042.

27. Kotake, C., Yamasaki, T., Moriyama, T., Shinoda, M., Komiyama, N., Furumai, T., Konishi, M., and Oki, T. (1992). Butyrolactols A and B, new antifungal antibiotics. Taxonomy, isolation, physico-chemical properties, structure and biological activity. J. Antibiot. (Tokyo) *45*, 1442–1450. https://doi.org/10.7164/antibiotics.45.1442.

28. Komaki, H., Ichikawa, N., Hosoyama, A., Fujita, N., and Igarashi, Y. (2015). Draft genome sequence of *Streptomyces* sp. TP-A0882 reveals putative butyrolactol biosynthetic pathway. FEMS Microbiol. Lett. *362*, fnv155. https://doi.org/10.1093/femsle/fnv155.

29. Gomez-Escribano, J.P., and Bibb, M.J. (2011). Engineering Streptomyces coelicolor for heterologous expression of secondary metabolite gene clusters. Microb. Biotechnol. *4*, 207–215. https://doi.org/10.1111/j.1751-7915.2010.00219.x.

30. Ogawa, H., Iwasaki, A., Sumimoto, S., Kanamori, Y., Ohno, O., Iwatsuki, M., Ishiyama, A., Hokari, R., Otoguro, K., O□mura, S., et al. (2016). Janadolide, a Cyclic Polyketide–Peptide Hybrid Possessing a tert-Butyl Group from an Okeania sp. Marine Cyanobacterium. J. Nat. Prod. *79*, 1862–1866. https://doi.org/10.1021/acs.jnatprod.6b00171.

31. Harunari, E., Komaki, H., and Igarashi, Y. (2017). Biosynthetic origin of butyrolactol A, an antifungal polyketide produced by a marine-derived *Streptomyces*. Beilstein J. Org. Chem. *13*, 441–450. https://doi.org/10.3762/bjoc.13.47.

32. Skiba, M.A., Sikkema, A.P., Moss, N.A., Tran, C.L., Sturgis, R.M., Gerwick, L., Gerwick, W.H., Sherman, D.H., and Smith, J.L. (2017). A Mononuclear Iron-Dependent Methyltransferase Catalyzes Initial Steps in Assembly of the Apratoxin A Polyketide Starter Unit. ACS Chem. Biol. *12*, 3039–3048. https://doi.org/10.1021/acschembio.7b00746.

33. Mirdita, M., Schütze, K., Moriwaki, Y., Heo, L., Ovchinnikov, S., and Steinegger, M. (2022). ColabFold: making protein folding accessible to all. Nat. Methods *19*, 679–682. https://doi.org/10.1038/s41592-022-01488-1.

34. Hong, H.-J., Hutchings, M.I., Hill, L.M., and Buttner, M.J. (2005). The Role of the Novel Fem Protein VanK in Vancomycin Resistance in *Streptomyces coelicolor**. J. Biol. Chem. *280*, 13055–13061. https://doi.org/10.1074/jbc.M413801200.

35. Sabino, R., Veríssimo, C., Pereira, Á.A., and Antunes, F. (2020). Candida auris, an Agent of Hospital-Associated Outbreaks: Which Challenging Issues Do We Need to Have in Mind? Microorganisms *8*, E181. https://doi.org/10.3390/microorganisms8020181.

36. Eyre, D.W., Sheppard, A.E., Madder, H., Moir, I., Moroney, R., Quan, T.P., Griffiths, D., George, S., Butcher, L., Morgan, M., et al. (2018). A Candida auris Outbreak and Its Control in an Intensive Care Setting. N. Engl. J. Med. *379*, 1322–1331. https://doi.org/10.1056/NEJMoa1714373.

37. Fuchs, B.B., O'Brien, E., El Khoury, J.B., and Mylonakis, E. (2010). Methods for using Galleria mellonella as a model host to study fungal pathogenesis. Virulence *1*, 475–482. https://doi.org/10.4161/viru.1.6.12985.

38. Kim, G.H., Rosiana, S., Kirienko, N.V., and Shapiro, R.S. (2020). A Simple Nematode Infection Model for Studying Candida albicans Pathogenesis. Curr. Protoc. Microbiol. *59*, e114. https://doi.org/10.1002/cpmc.114.

39. Vincent, B.M., Lancaster, A.K., Scherz-Shouval, R., Whitesell, L., and Lindquist, S. (2013). Fitness trade-offs restrict the evolution of resistance to amphotericin B. PLoS Biol. *11*, e1001692. https://doi.org/10.1371/journal.pbio.1001692.

40. Forastiero, A., Mesa-Arango, A.C., Alastruey-Izquierdo, A., Alcazar-Fuoli, L., Bernal-Martinez, L., Pelaez, T., Lopez, J.F., Grimalt, J.O., Gomez-Lopez, A., Cuesta, I., et al. (2013). Candida tropicalis Antifungal Cross-Resistance Is Related to Different Azole Target (Erg11p) Modifications. Antimicrob. Agents Chemother. *57*, 4769–4781. https://doi.org/10.1128/AAC.00477-13.

41. Anderson, T.M., Clay, M.C., Cioffi, A.G., Diaz, K.A., Hisao, G.S., Tuttle, M.D., Nieuwkoop, A.J., Comellas, G., Maryum, N., Wang, S., et al. (2014). Amphotericin forms an extramembranous and fungicidal sterol sponge. Nat. Chem. Biol. *10*, 400–406. https://doi.org/10.1038/nchembio.1496.

42. Anderson, J.B. (2005). Evolution of antifungal-drug resistance: mechanisms and pathogen fitness. Nat. Rev. Microbiol. *3*, 547–556. https://doi.org/10.1038/nrmicro1179.

43. Hu, G., and Kronstad, J.W. (2010). A Putative P-Type ATPase, Apt1, Is Involved in Stress Tolerance and Virulence in *Cryptococcus neoformans*. Eukaryot. Cell *9*, 74–83. https://doi.org/10.1128/EC.00289-09.

44. Hu, G., Caza, M., Bakkeren, E., Kretschmer, M., Bairwa, G., Reiner, E., and Kronstad, J. (2017). A P4-ATPase subunit of the Cdc50 family plays a role in iron acquisition and virulence in *Cryptococcus neoformans*. Cell. Microbiol. *19*, e12718. https://doi.org/10.1111/cmi.12718.

45. Stanchev, L.D., Rizzo, J., Peschel, R., Pazurek, L.A., Bredegaard, L., Veit, S., Laerbusch, S., Rodrigues, M.L., López-Marqués, R.L., and Günther Pomorski, T. (2021). P-Type ATPase Apt1 of the Fungal Pathogen Cryptococcus neoformans Is a Lipid Flippase of Broad Substrate Specificity. J. Fungi *7*, 843. https://doi.org/10.3390/jof7100843.

46. López-Marqués, R.L., Gourdon, P., Günther Pomorski, T., and Palmgren, M. (2020). The transport mechanism of P4 ATPase lipid flippases. Biochem. J. *477*, 3769–3790. https://doi.org/10.1042/BCJ20200249.

47. Pomorski, T., Lombardi, R., Riezman, H., Devaux, P.F., van Meer, G., and Holthuis, J.C.M. (2003). Drs2p-related P-type ATPases Dnf1p and Dnf2p Are Required for Phospholipid Translocation across the Yeast Plasma Membrane and Serve a Role in Endocytosis. Mol. Biol. Cell *14*, 1240–1254. https://doi.org/10.1091/mbc.e02-08-0501.

48. Duan, H.D., and Li, H. (2024). Consensus, controversies, and conundrums of P4-ATPases: The emerging face of eukaryotic lipid flippases. J. Biol. Chem. *300*, 107387. https://doi.org/10.1016/j.jbc.2024.107387.

49. Baldridge, R.D., and Graham, T.R. (2013). Two-gate mechanism for phospholipid selection and transport by type IV P-type ATPases. Proc. Natl. Acad. Sci. *110*. https://doi.org/10.1073/pnas.1216948110.

50. Richter, M.F., Drown, B.S., Riley, A.P., Garcia, A., Shirai, T., Svec, R.L., and Hergenrother, P.J. (2017). Predictive compound accumulation rules yield a broad-spectrum antibiotic. Nature *545*, 299–304. https://doi.org/10.1038/nature22308.

51. Saito, K., Fujimura-Kamada, K., Furuta, N., Kato, U., Umeda, M., and Tanaka, K. (2004). Cdc50p, a Protein Required for Polarized Growth, Associates with the Drs2p P-Type ATPase Implicated in Phospholipid Translocation in *Saccharomyces cerevisiae*. Mol. Biol. Cell *15*, 3418–3432. https://doi.org/10.1091/mbc.e03-11-0829.

52. Chen, S., Wang, J., Muthusamy, B.-P., Liu, K., Zare, S., Andersen, R.J., and Graham, T.R. (2006). Roles for the Drs2p-Cdc50p Complex in Protein Transport and Phosphatidylserine Asymmetry of the Yeast Plasma Membrane. Traffic *7*, 1503–1517. https://doi.org/10.1111/j.1600-0854.2006.00485.x.

53. Hua, Z., Fatheddin, P., and Graham, T.R. (2002). An essential subfamily of Drs2p-related P-type ATPases is required for protein trafficking between Golgi complex and endosomal/vacuolar system. Mol. Biol. Cell *13*, 3162–3177. https://doi.org/10.1091/mbc.e02-03-0172.

54. Liu, K., Hua, Z., Nepute, J.A., and Graham, T.R. (2007). Yeast P4-ATPases Drs2p and Dnf1p are essential cargos of the NPFXD/Sla1p endocytic pathway. Mol. Biol. Cell *18*, 487–500. https://doi.org/10.1091/mbc.e06-07-0592.

55. Liu, K., Surendhran, K., Nothwehr, S.F., and Graham, T.R. (2008). P4-ATPase Requirement for AP-1/Clathrin Function in Protein Transport from the *trans* -Golgi Network and Early Endosomes. Mol. Biol. Cell *19*, 3526–3535. https://doi.org/10.1091/mbc.e08-01-0025.

56. Nakanishi, H., Nishizawa, T., Segawa, K., Nureki, O., Fujiyoshi, Y., Nagata, S., and Abe, K. (2020). Transport Cycle of Plasma Membrane Flippase ATP11C by Cryo-EM. Cell Rep. *32*. https://doi.org/10.1016/j.celrep.2020.108208.

57. Hiraizumi, M., Yamashita, K., Nishizawa, T., and Nureki, O. (2019). Cryo-EM structures capture the transport cycle of the P4-ATPase flippase. Science *365*, 1149–1155. https://doi.org/10.1126/science.aay3353.

58. Dieudonné, T., Kümmerer, F., Laursen, M.J., Stock, C., Flygaard, R.K., Khalid, S., Lenoir, G., Lyons, J.A., Lindorff-Larsen, K., and Nissen, P. (2023). Activation and substrate specificity of the human P4-ATPase ATP8B1. Nat. Commun. *14*, 7492. https://doi.org/10.1038/s41467-023-42828-9.

59. Bai, L., You, Q., Jain, B.K., Duan, H.D., Kovach, A., Graham, T.R., and Li, H. (2020). Transport mechanism of P4 ATPase phosphatidylcholine flippases. eLife *9*, e62163. https://doi.org/10.7554/eLife.62163.

60. Xu, J., He, Y., Wu, X., and Li, L. (2022). Conformational changes of a phosphatidylcholine flippase in lipid membranes. Cell Rep. *38*, 110518. https://doi.org/10.1016/j.celrep.2022.110518.

61. Wang, Y., Lyons, J.A., Timcenko, M., Kümmerer, F., Groot, B.L. de, Nissen, P., Gapsys, V., and Lindorff-Larsen, K. (2021). Substrate Transport and Specificity in a Phospholipid Flippase. Preprint at bioRxiv, https://doi.org/10.1101/2020.06.24.169771 https://doi.org/10.1101/2020.06.24.169771.

62. Chalat, M., Moleschi, K., and Molday, R.S. (2017). C-terminus of the P4-ATPase ATP8A2 functions in protein folding and regulation of phospholipid flippase activity. Mol. Biol. Cell *28*, 452–462. https://doi.org/10.1091/mbc.E16-06-0453.

63. Fan, Y., and Lin, X. (2018). Multiple Applications of a Transient CRISPR-Cas9 Coupled with Electroporation (TRACE) System in the Cryptococcus neoformans Species Complex. Genetics *208*, 1357–1372. https://doi.org/10.1534/genetics.117.300656.

64. Rizzo, J., Colombo, A.C., Zamith-Miranda, D., Silva, V.K.A., Allegood, J.C., Casadevall, A., Del Poeta, M., Nosanchuk, J.D., Kronstad, J.W., and Rodrigues, M.L. (2018). The putative flippase Apt1 is required for intracellular membrane architecture and biosynthesis of polysaccharide and lipids in Cryptococcus neoformans. Biochim. Biophys. Acta BBA - Mol. Cell Res. *1865*, 532–541. https://doi.org/10.1016/j.bbamcr.2017.12.007.

65. Chen, C.-Y., Ingram, M.F., Rosal, P.H., and Graham, T.R. (1999). Role for Drs2p, a P-Type Atpase and Potential Aminophospholipid Translocase, in Yeast Late Golgi Function. J. Cell Biol. *147*, 1223–1236. https://doi.org/10.1083/jcb.147.6.1223.

66. Novick, P., Field, C., and Schekman, R. (1980). Identification of 23 complementation groups required for post-translational events in the yeast secretory pathway. Cell *21*, 205–215. https://doi.org/10.1016/0092-8674(80)90128-2.

67. Roemer, T., Jiang, B., Davison, J., Ketela, T., Veillette, K., Breton, A., Tandia, F., Linteau, A., Sillaots, S., Marta, C., et al. (2003). Large-scale essential gene identification in Candida albicans and applications to antifungal drug discovery. Mol. Microbiol. *50*, 167–181. https://doi.org/10.1046/j.1365-2958.2003.03697.x.

68. Gurunathan, S. (2002). Dynamin and clathrin are required for the biogenesis of a distinct class of secretory vesicles in yeast. EMBO J. *21*, 602–614. https://doi.org/10.1093/emboj/21.4.602.

69. Wendland, B., and Emr, S.D. (1998). Pan1p, yeast eps15, functions as a multivalent adaptor that coordinates protein-protein interactions essential for endocytosis. J. Cell Biol. *141*, 71–84. https://doi.org/10.1083/jcb.141.1.71.

70. Vida, T.A., and Emr, S.D. (1995). A new vital stain for visualizing vacuolar membrane dynamics and endocytosis in yeast. J. Cell Biol. *128*, 779–792. https://doi.org/10.1083/jcb.128.5.779.

71. Sekiya-Kawasaki, M., Groen, A.C., Cope, M.J.T.V., Kaksonen, M., Watson, H.A., Zhang, C., Shokat, K.M., Wendland, B., McDonald, K.L., McCaffery, J.M., et al. (2003). Dynamic phosphoregulation of the cortical actin cytoskeleton and endocytic machinery revealed by real-time chemical genetic analysis. J. Cell Biol. *162*, 765–772. https://doi.org/10.1083/jcb.200305077.

72. Kishimoto, T., Yamamoto, T., and Tanaka, K. (2005). Defects in Structural Integrity of Ergosterol and the Cdc50p-Drs2p Putative Phospholipid Translocase Cause Accumulation of Endocytic

Membranes, onto Which Actin Patches Are Assembled in Yeast. Mol. Biol. Cell *16*, 5592–5609. https://doi.org/10.1091/mbc.e05-05-0452.

73. Epp, E., Nazarova, E., Regan, H., Douglas, L.M., Konopka, J.B., Vogel, J., and Whiteway, M. (2013). Clathrin- and Arp2/3-Independent Endocytosis in the Fungal Pathogen Candida albicans. mBio *4*, 10.1128/mbio.00476-13. https://doi.org/10.1128/mbio.00476-13.

74. Auland, M.E., Roufogalis, B.D., Devaux, P.F., and Zachowski, A. (1994). Reconstitution of ATP-dependent aminophospholipid translocation in proteoliposomes. Proc. Natl. Acad. Sci. U. S. A. *91*, 10938–10942. https://doi.org/10.1073/pnas.91.23.10938.

75. Muthusamy, B.-P., Natarajan, P., Zhou, X., and Graham, T.R. (2009). Linking phospholipid flippases to vesicle-mediated protein transport. Biochim. Biophys. Acta BBA - Mol. Cell Biol. Lipids *1791*, 612–619. https://doi.org/10.1016/j.bbalip.2009.03.004.

76. Gall, W.E., Geething, N.C., Hua, Z., Ingram, M.F., Liu, K., Chen, S.I., and Graham, T.R. (2002). Drs2p-Dependent Formation of Exocytic Clathrin-Coated Vesicles In Vivo. Curr. Biol. *12*, 1623–1627. https://doi.org/10.1016/S0960-9822(02)01148-X.

77. Das, A., Slaughter, B.D., Unruh, J.R., Bradford, W.D., Alexander, R., Rubinstein, B., and Li, R. (2012). Flippase-mediated phospholipid asymmetry promotes fast Cdc42 recycling in dynamic maintenance of cell polarity. Nat. Cell Biol. *14*, 304–310. https://doi.org/10.1038/ncb2444.

78. Verhulst, P.M., van der Velden, L.M., Oorschot, V., van Faassen, E.E., Klumperman, J., Houwen, R.H.J., Pomorski, T.G., Holthuis, J.C.M., and Klomp, L.W.J. (2010). A flippase-independent function of ATP8B1, the protein affected in familial intrahepatic cholestasis type 1, is required for apical protein expression and microvillus formation in polarized epithelial cells. Hepatol. Baltim. Md *51*, 2049–2060. https://doi.org/10.1002/hep.23586.

79. Rizzo, J., Oliveira, D.L., Joffe, L.S., Hu, G., Gazos-Lopes, F., Fonseca, F.L., Almeida, I.C., Frases, S., Kronstad, J.W., and Rodrigues, M.L. (2014). Role of the Apt1 Protein in Polysaccharide Secretion by Cryptococcus neoformans. Eukaryot. Cell *13*, 715–726. https://doi.org/10.1128/EC.00273-13.

80. Pommier, Y. (2006). Topoisomerase I inhibitors: camptothecins and beyond. Nat. Rev. Cancer *6*, 789–802. https://doi.org/10.1038/nrc1977.

81. Huai, Q., Kim, H.-Y., Liu, Y., Zhao, Y., Mondragon, A., Liu, J.O., and Ke, H. (2002). Crystal structure of calcineurin–cyclophilin–cyclosporin shows common but distinct recognition of immunophilin–drug complexes. Proc. Natl. Acad. Sci. U. S. A. *99*, 12037. https://doi.org/10.1073/pnas.192206699.

82. Rivera, A., and Heitman, J. (2023). Natural product ligands of FKBP12: Immunosuppressive antifungal agents FK506, rapamycin, and beyond. PLOS Pathog. *19*, e1011056. https://doi.org/10.1371/journal.ppat.1011056.

83. Lorenz, M.C., and Heitman, J. (1995). TOR Mutations Confer Rapamycin Resistance by Preventing Interaction with FKBP12-Rapamycin (*). J. Biol. Chem. *270*, 27531–27537. https://doi.org/10.1074/jbc.270.46.27531.

84. Structure of the FKBP12-Rapamycin Complex Interacting with Binding Domain of Human FRAP | Science https://www.science.org/doi/10.1126/science.273.5272.239.

85. Pianalto, K.M., Billmyre, R.B., Telzrow, C.L., and Alspaugh, J.A. (2019). Roles for Stress Response and Cell Wall Biosynthesis Pathways in Caspofungin Tolerance in Cryptococcus neoformans. Genetics *213*, 213–227. https://doi.org/10.1534/genetics.119.302290.

Figure

Figure 1

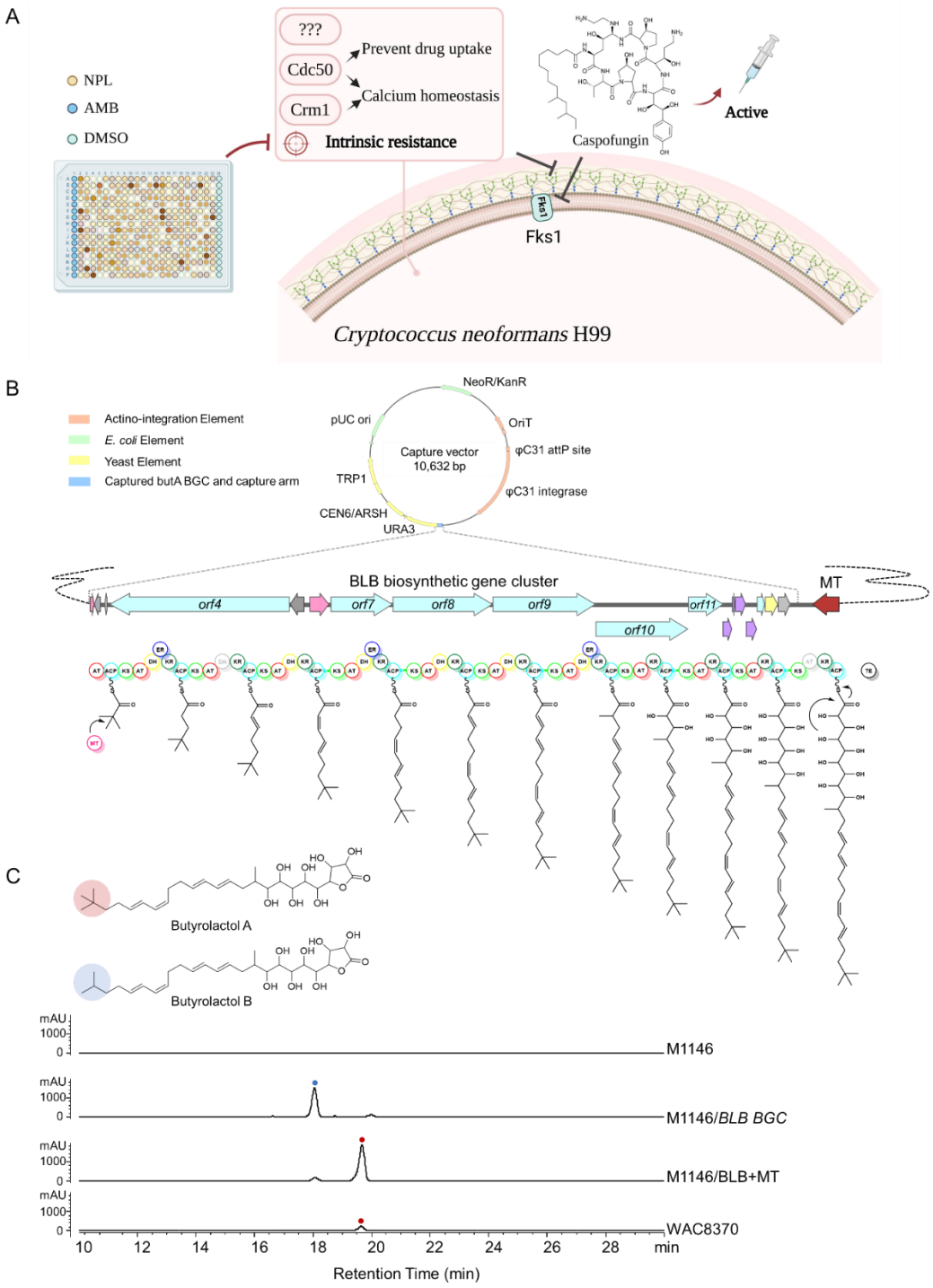

Figure 1. A high throughput screen for potentiators of caspofungin against *Cryptococcus neoformans* H99 and the high-yield biosynthetic producers of butyrolactol A and B.

(A) Overview of the screening strategy using the natural product library (NPL) to identify caspofungin potentiators that can overcome intrinsic resistance in *Cryptococcus* species. Amphotericin B (AMB) as a positive antifungal control. See also Figure S1.
(B) Identification and capture of the butyrolactol B (BLB) biosynthetic gene cluster (BGC) and C-methyltransferase from the genome of *Streptomyces ardesiacus* WAC8370. The organization of BLB BGC is color-coded: blue for polyketide backbone (PKS), purple for hydroxymalonyl-ACP biosynthesis genes, pink for the transcriptional regulator, light yellow for the transporter, and red for methyltransferase (MT). PKS domains are labeled as follows: AT, acyltransferase; KS, keto synthase; ACP, acyl carrier protein; KR, ketoreductase; DH, dehydratase; ER, enoylreductase; MT, methyltransferase TE, thioesterase. The transformation-associated recombination-based BGC capture, and the following heterologous strategy are presented in Figure S2D. See also Tables S1. (C) Chromatographic analysis of butyrolactol A (BLA) and butyrolactol B (BLB) produced by heterologous hosts, compared to the natural producer *S. ardesiacus* WAC8370. BLA and BLB are marked with red and blue dots, respectively, with differentiated terminal structures shown in corresponding colors. M1146 refers to *S. coelicolor* M1146; M1146/BLB contains the butyrolactol B biosynthetic gene cluster; and M1146/BLB+MT includes both the BLB gene cluster and the methyltransferase. See also Figure S2

Figure 2

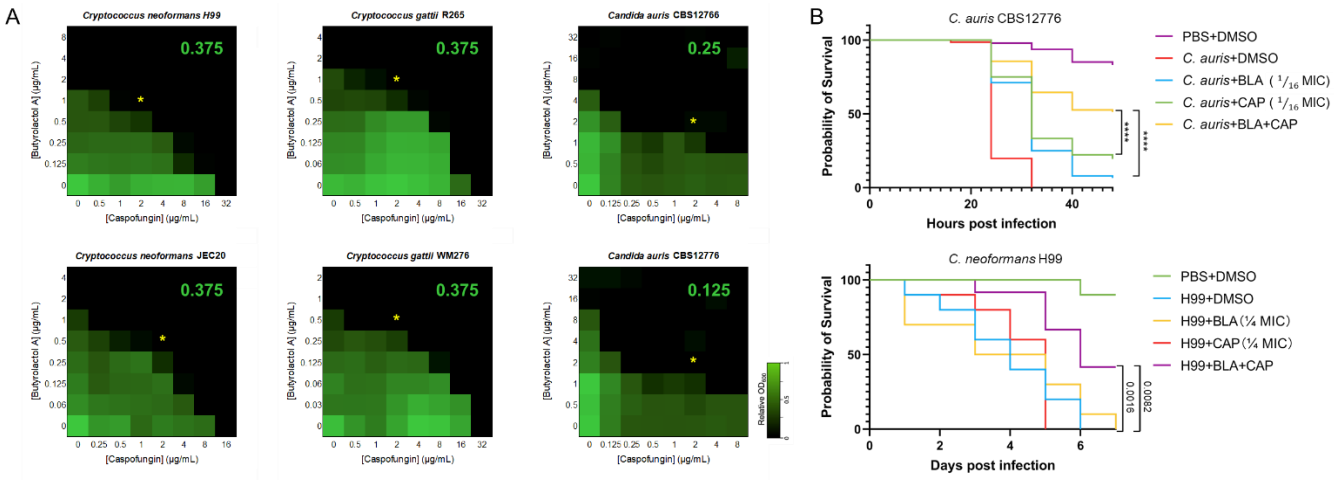

Figure 2. Butyrolactol A synergizes with caspofungin in *Cryptococcus* spp. and resistant *Candida auris.*

(A) Checkerboard assays depicted as heatmaps show the average growth of biological duplicates, normalized to no compound controls. Compound potentiation was assessed against *Cryptococcus neoformans* H99 and JEC20, *Cryptococcus gattii* R265 and WM276, and *Candida auris* CBS12766 and CBS12776. Relative growth is quantitatively represented by color (see scale bar at the bottom right). Fractional Inhibitory Concentration Index (FICI) values were calculated as described in the methods and are displayed in the top right corner of each checkerboard. FICI values below 0.5 indicate synergistic interactions. The yellow asterisk highlights the rescue concentration of butyrolactol A (BLA), which reduces the minimum inhibitory concentration (MIC) of caspofungin to the clinical breakpoint (2 µg/mL). (B) *C. elegans* were infected with *C. auris* CBS 12766 (upper) and *G. mellonella* were infected with *C. neoformans* H99 (bottom). Survival was monitored in the presence of butyrolactol A (BLA), caspofungin (CAP), the combination of both, or without treatment. For each condition, 20 *C. elegans* worms were used, and survival was tracked over 48 hours across 3 independent trials. Similarly, 10 *G. mellonella* larvae were used for each condition, and survival was tracked over seven days after injection with ~10^6 per larvae in 3 independent trials. Survival was plotted using a Kaplan-Meier survival curve. Significance was determined using the Log-rank (Mantel-Cox) test, comparing monotherapy of CAP (left) and BLA (right) to combination therapy, with the corresponding p-values indicated as numerical values or **** for $p < 0.0001$.

Figure 3

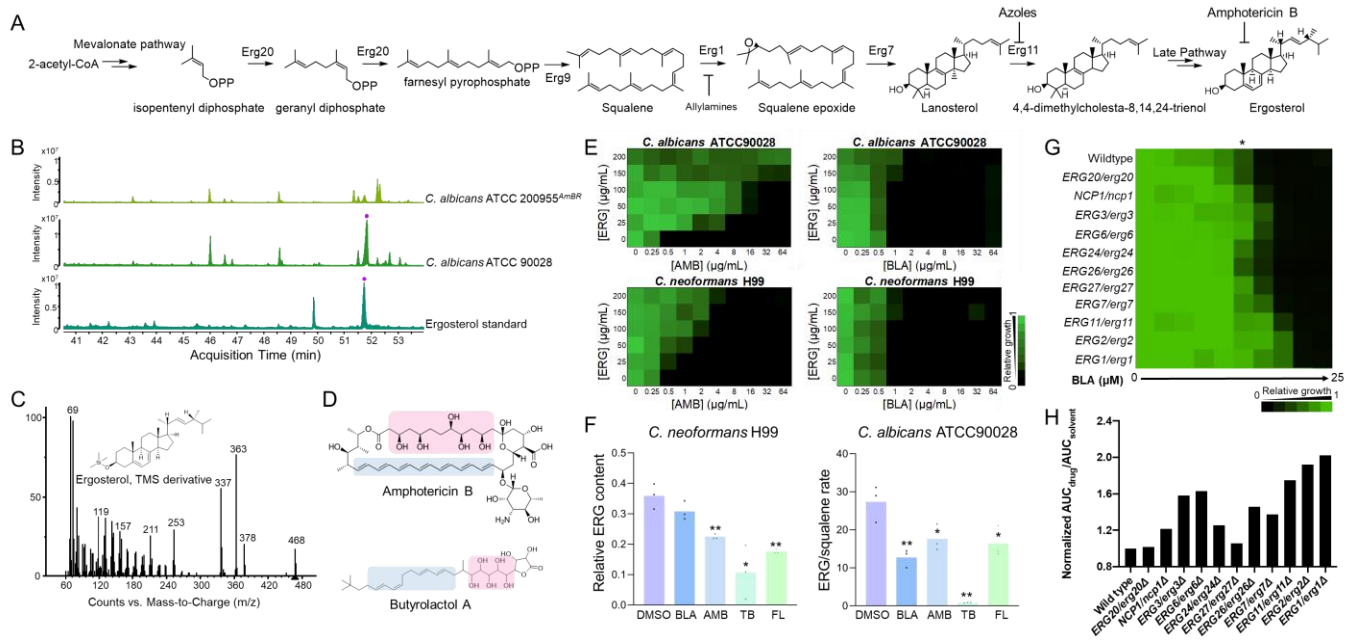

Figure 3. Butyrolactol A perturbs sterol homeostasis but does not target ergosterol or its biosynthesis.

(A) Simplified schematic of the ergosterol biosynthesis pathway, along with antifungals targeting ergosterol or its biosynthesis. (B) Gas chromatography-mass spectrometry (GC-MS) analysis of ergosterol in amphotericin B-resistant *C. albicans* ATCC200955 (upper) and amphotericin B-sensitive *C. albicans* ATCC90028 (middle). The ergosterol standard is shown as a reference (bottom). (C) Chemical structure and GC-MS spectrum of ergosterol-TMS derivative. (D) Structural comparison of butyrolactol A and amphotericin B, highlighting structural similarities. The hydrophobic polyene region is indicated in blue, while the hydrophilic polyol structure is in pink. (E) Rescue effect of exogenous ergosterol (ERG) on cell viability during treatment with butyrolactol A (BLA), with amphotericin B (AMB) used as a positive control. Two-fold serial dilutions of ergosterol were added to *C. neoformans* H99 and *C. albicans* ATCC90028 in the presence of AMB or BLA, respectively. Biological duplicates were averaged and normalized to no-drug and no-ergosterol controls. Relative growth is quantitatively represented by color (see scale bar at the bottom right). (F) Relative ergosterol (ERG) abundance in *C. neoformans* H99 and *C. albicans* ATCC90028, treated or untreated with butyrolactol A and different agents targeting ergosterol biosynthesis: amphotericin B (AMB), terbinafine (TB), and fluconazole (FL). The median value of three biological replicates is represented by the height of each bar, with individual experimental values indicated by dots. Significance was determined by one-way ANOVA with Dunnett's multiple comparisons test, comparing each treatment to the untreated control (* $p < 0.05$, ** $p < 0.01$, t-test). (G) *In vitro* susceptibility of *C. albicans* wild-type (WT) and heterozygous-deletion mutants to BLA. Dose-response assays were performed in YPD medium, with growth measured by absorbance at 600 nm after 24 hours at 30°C. Optical

densities were averaged from duplicate measurements and normalized to the growth of untreated WT strains. Results are depicted as in Figure 2A (see bar for scale). (* indicates concentrations selected for plotting the growth curve). (H) Relative growth of *C. albicans* strains at 1.56 μM BLA (indicated by * in Figure 3G). The area under the growth curve (AUC) for strains in the presence of BLA was normalized to their AUC in the absence of BLA to eliminate baseline growth discrepancies. Data are presented as the mean of technical replicates.

Figure 4

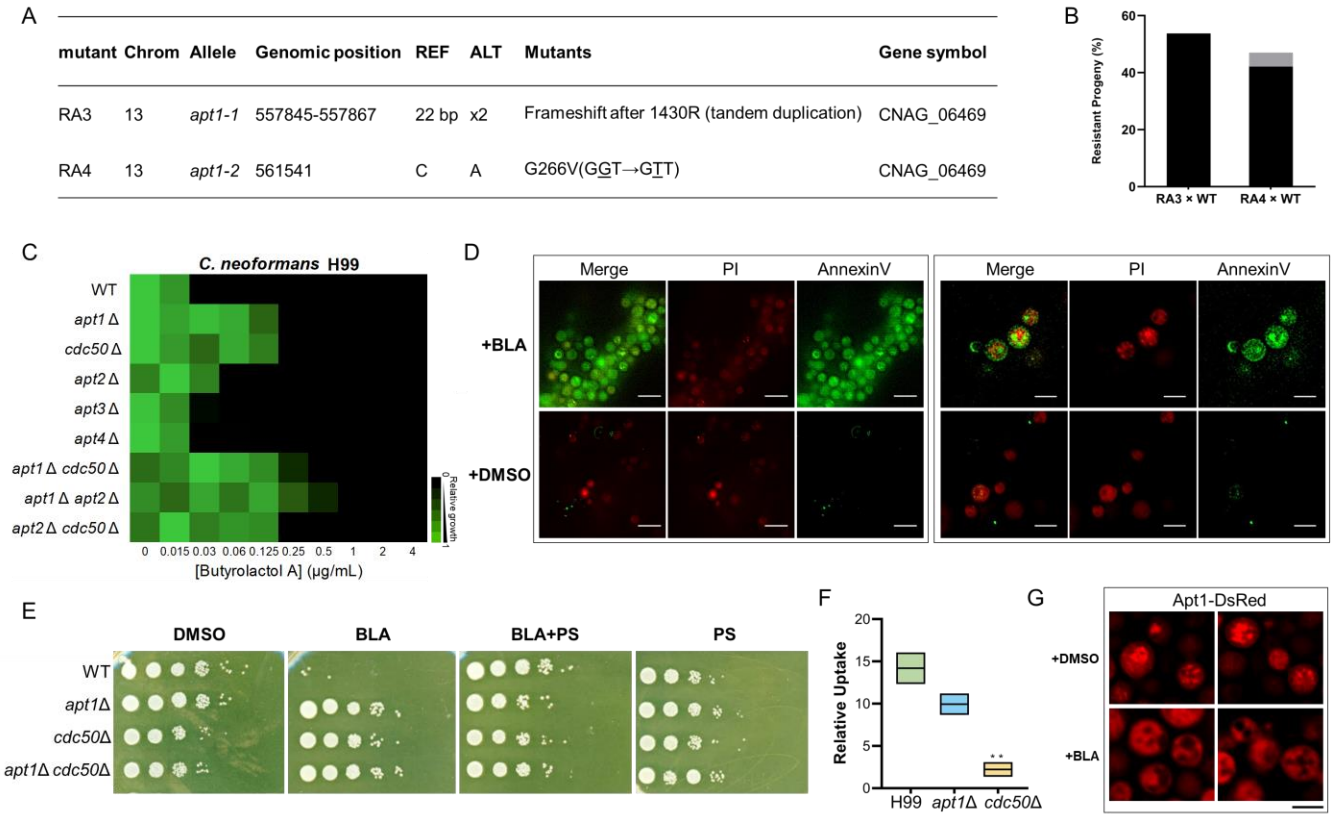

Figure 4. Identification of butyrolactol A as a novel inhibitor of the flippase complex Apt1–Cdc50.

(A) Genotypes of BLA-resistant mutants, carrying mutations in *APT1* (*CNAG_06469*). See also BLA susceptibility results in Figure S3A. (B) Results of the genetic cross between BLA-resistant mutants and the wild-type strain (KN99**a**). The *y*-axis represents the percentage of resistant progeny, with the inherited resistant genotypes from the parent strains shown in black. The *x*-axis shows different cross tests between independent resistant mutants RA3 and RA4 (as mentioned in Figure 4A) and the wild-type strain KN99a (WT). See also Table S4. (C) Dose-response assays were performed against wild-type *C. neoformans* (H99) and various flippase-compromised mutants. Growth was measured using absorbance at 530 nm in SDB medium at 30 °C after 48 hours. Growth relative to untreated wild-type control wells is presented in a

heatmap format (see scale bar). Each colored box represents the mean of duplicate experiments. (D) *C. neoformans* H99 cells in log phase were treated with BLA (upper) or an equivalent amount of DMSO (bottom) and were co-incubated with Annexin V Alexa Fluor™ 488 and Propidium Iodide (PI), then observed using fluorescence microscopy. The Annexin V Alexa Fluor™ 488 signal was detected in the FITC channel, and the PI signal was detected in the TexRed channel. Scale bars are shown in each image: 10 μm (left column) and 5 μm (right column). (E) The effect of exogenous phosphatidylserine (PS) on the viability of wild-type *C. neoformans* H99, *apt1*Δ, *cdc50*Δ, and *apt1*Δ *cdc50*Δ mutants in the presence or absence of BLA. Strains were inoculated in SDB medium treated with BLA, PS, or a combination of BLA and PS for 24 hours. Equivalent vehicle DMSO was used as a control. Ten-fold serial dilutions of the 24-hour cultures were spotted onto yeast extract peptone dextrose (YPD) plates. Plates were incubated at 30 °C for 2 days before imaging. (F) The relative intracellular concentrations of BLA accumulated in *C. neoformans* H99 and *apt1*Δ and *cdc50*Δ mutants were measured after 15 minutes of treatment. Data are presented as mean ± SD of biological triplicates. Statistical significance was determined using multiple unpaired t-tests with Holm-Sidak's multiple comparisons correction, comparing all conditions to wild-type H99. p-values: ** <0.01. (G) Localization of DsRed-Apt1p in *C. neoformans* H99 cells with (upper row) and without (lower row) BLA treatment. Representative fluorescence confocal images were taken in the TexRed channel. Scale bar, 5 μm.

Figure 5

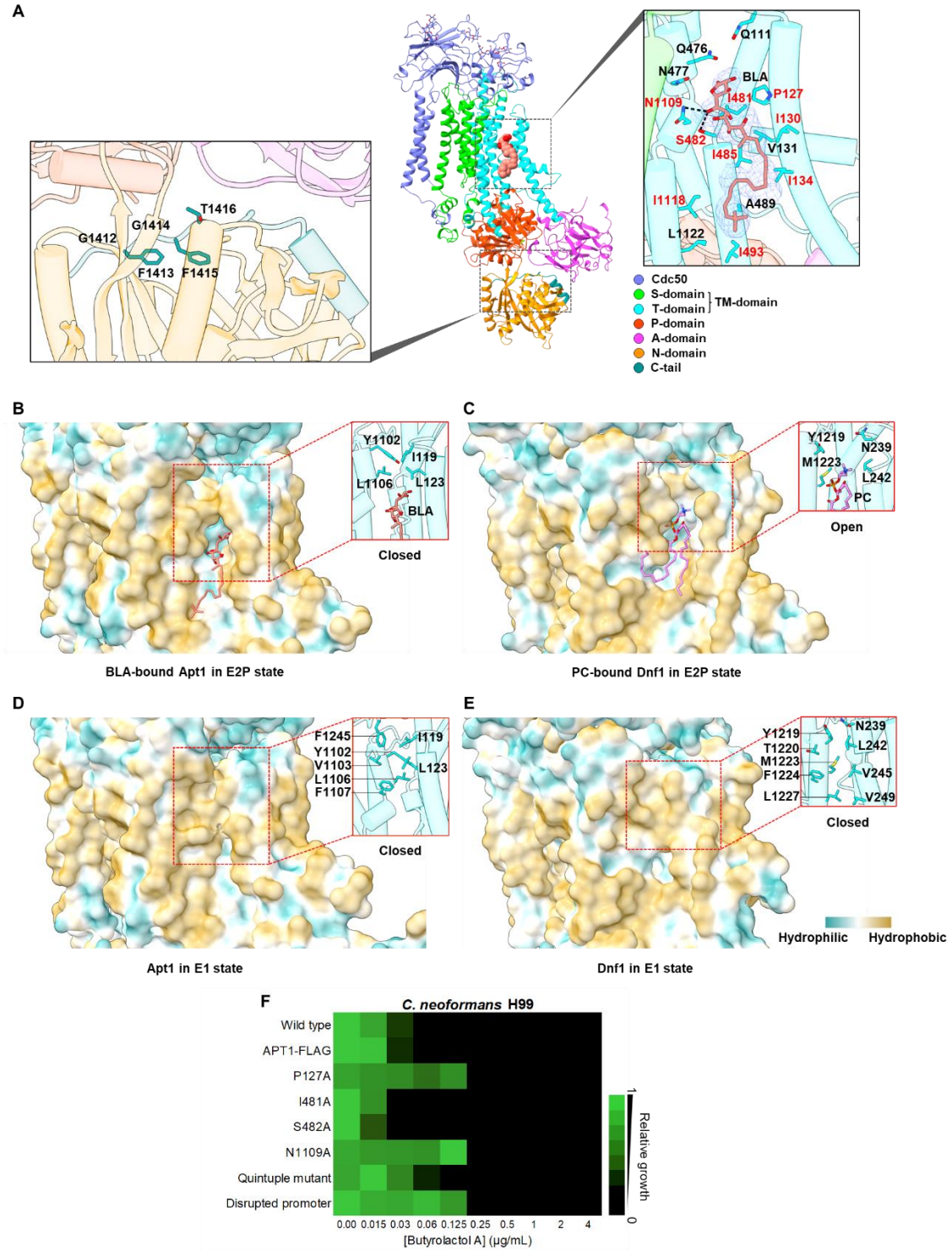

Figure 5. Cryo-EM Reveals butyrolactol A Binding to Apt1–Cdc50 and Obstruction of the Lipid Transport Channel.

(A) Overall structure (middle) of *C. neoformans* Apt1–Cdc50 bound with BLA (salmon spheres) in the E2P state with major domains shown in different colors. TM-domain, transmembrane domain; S-domain, support domain; T-domain, transport domain; P-domain, phosphorylation domain; A-domain, actuator domain; N-domain, nucleotide-binding domain. Left: enlarged view of the autoregulatory C-tail with the GFGFT motif shown in teal sticks. Right: enlarged view of BLA binding site with the EM density of BLA superimposed on the atomic model and shown as blue mesh. BLA and residues surrounding the BLA binding site are shown in sticks. The key residues forming either H-bonds (indicated by dashed line with a cutoff distance of 3.5 Å) or hydrophobic interactions (cutoff distance: 4.0 Å) with BLA are labeled in red. (B) Binding of BLA to Apt1 in the E2P state induces closure of the lipid entry site shown in hydrophobicity surface. BLA is shown in salmon sticks and a cartoon representation of the lipid entry site boxed in red is also shown in the inset with the entry closing residues in cyan sticks. (C) Lipid entry site of *S. cerevisiae* Dnf1 in the E2P state remains open upon binding of the substrate lipid PC as shown in the hydrophobicity surface (PDB ID 7KYC). PC is shown in magenta sticks and a cartoon representation of the lipid entry site in the open state boxed in red is also shown in the inset. (D) Lipid entry site of Apt1 in the E1 state is closed as shown in the hydrophobicity surface (PDB ID 9DZV, this study). A cartoon representation of the closed lipid entry site boxed in red is also shown in the inset with interacting residues in cyan sticks. (E) The closed lipid entry site of *S. cerevisiae* Dnf1 in the E1 state as shown in the hydrophobicity surface (PDB ID 7KY6). A cartoon representation of the entry closing boxed in red is also shown in the inset with interacting residues in cyan sticks. (F) BLA susceptibility of wild-type *C. neoformans* H99 and various mutants, including FLAG-tagged Apt1 (Apt1-FLAG), single substitutions P127A, I481A, S482A, N1109A, a quintuple mutant (I130A, I134A, I485A, I493A, I1118A), and the Apt1-FLAG promoter disrupted mutant. Relative growth is shown in heat-map format (see scale bar). Each colored box represents the mean of duplicate measurements. Refer to the transcriptional and translational levels of Apt1 in wild-type and mutant strains in Figures S6B and S6C.

Figure 6

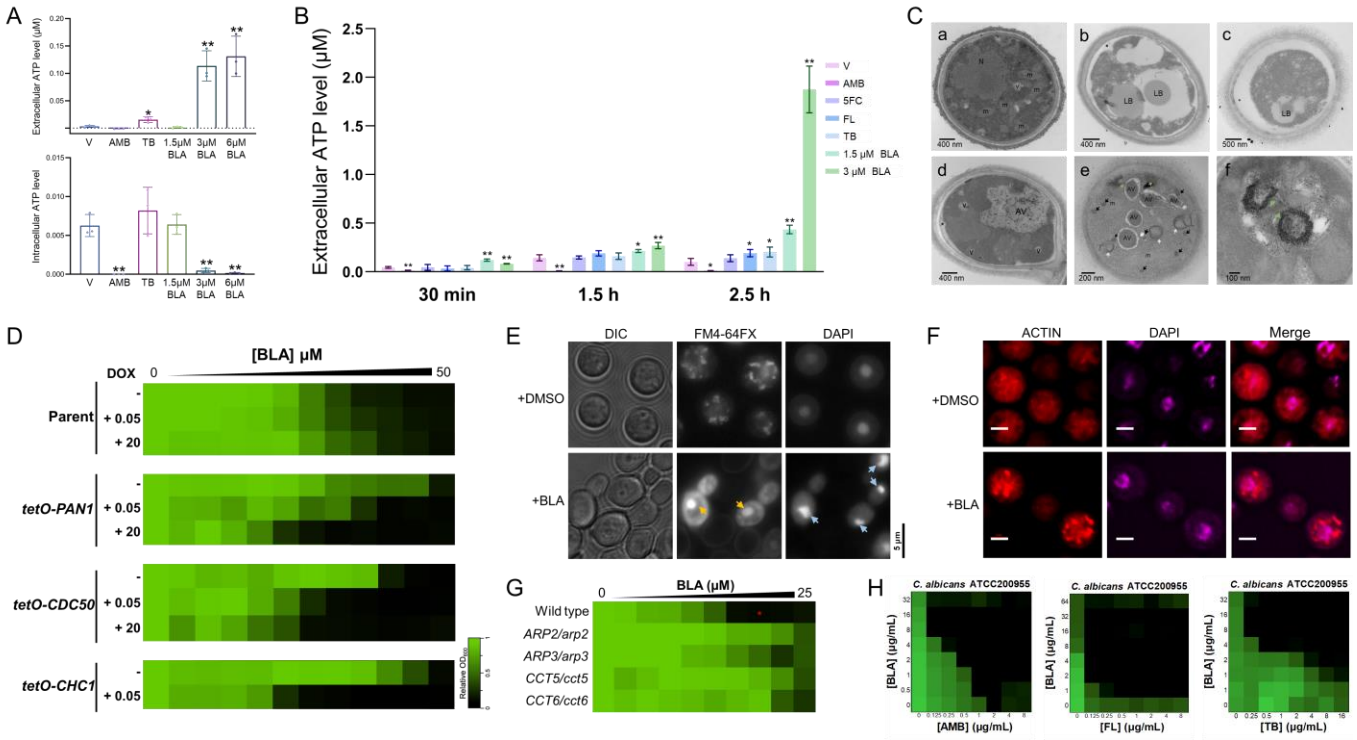

Figure 6. BLA inhibition of Apt1–Cdc50 disrupts membrane architecture and trafficking. (A) Cellular and extracellular ATP levels were measured following treatment. Log-phase *C. neoformans* H99 cells were cultured in SDB medium in the presence of amphotericin B (AMB), terbinafine (TB), butyrolactol A (BLA), or vehicle (-). Data are expressed as the mean ± SD of biological triplicates. Statistical significance was determined by multiple *t*-tests compared to the vehicle control (*$P < 0.05$, **$P < 0.01$). (B) ATP leakage was tracked by the extracellular ATP of *C. neoformans* H99 measured at 0.5-, 1.5-, and 2.5-hours post-treatment. 5-fluorocytosine (5FC), Fluconazole (FL). Experiments were performed in triplicate, and error bars represent standard deviations (n = 3). Statistical significance was assessed by multiple *t*-tests, with significance denoted by asterisks (*$P < 0.05$, **$P < 0.01$) for each treatment compared to the vehicle control. (C) *C. neoformans* accumulates abnormal membrane structures following BLA treatment. Cells were grown in SDB medium with BLA or vehicle, fixed, and visualized using transmission electron microscopy (TEM). Vehicle (DMSO) treated cells are shown in (a), while cells treated with 1 μM BLA are displayed in (b-d), and cells treated with 0.5 μM BLA in (e-f), with (f) showing a magnified view. Membrane defects in BLA-treated cells include enlarged atypical vacuoles (AV), double-membrane rings, crescent-shaped structures (white arrowheads), accumulated vesicles (black arrowheads), electron-dense misfolded membranes (green arrowheads), lipid bodies (LB), nuclei (N), mitochondria (M), and vacuoles (V). (D) BLA two-fold dose-response assays were conducted using wild-type and conditional expression *C. albicans* strains of *PAN1* (tetO-*PAN1/pan1*Δ), *CDC50* (tetO-*CDC50/cdc50*Δ), and *CHC1* (tetO-

*CHC1/chc1*Δ) with varying concentrations of doxycycline (DOX, 0.05 µg/mL and 20 µg/mL). Growth was measured by absorbance at 600 nm after 48 hours at 30°C. Data are presented as a heatmap, with color representing relative growth, normalized to no-drug controls. (E) Endocytosis was assessed in *C. neoformans* H99 treated with or without BLA. Mid-log-phase cells were stained with FM 4-64 and DAPI, then visualized by fluorescence microscopy (100×). Yellow arrowheads indicate abnormal vacuoles/endosomes, and blue arrowheads indicate DAPI-stained nuclei. Scale bar (5 µm) is located at the bottom left. (F) The effect of BLA on actin cytoskeleton organization in *C. neoformans* H99 was examined by epifluorescence microscopy. Early-log-phase cells treated with low concentrations of BLA, or vehicle were fixed and stained with Alexa Fluor 568 phalloidin, and mounted with DAPI. Scale bar = 2 µm. (G) *In vitro* BLA susceptibility of *C. albicans* wild-type (WT) and heterozygous deletion mutants for genes involved in actin assembly. Dose-response assays were performed in YPD medium, with growth measured by absorbance at 600 nm after 24 hours at 30 °C. Data are depicted as in panel (D). (* indicates concentrations selected for growth curve plotting in Figure S7A). (H) Synergy plots for BLA in combination with drugs targeting ergosterol or its biosynthesis. Checkerboard assays, presented as heatmaps, show the average growth inhibition of *C. albicans* ATCC200955 across biological triplicates, normalized to no-compound controls. Fractional Inhibitory Concentration Index (FICI) values are shown in the top right of each heatmap, with values <0.5 indicating synergistic interactions.

Figure 7

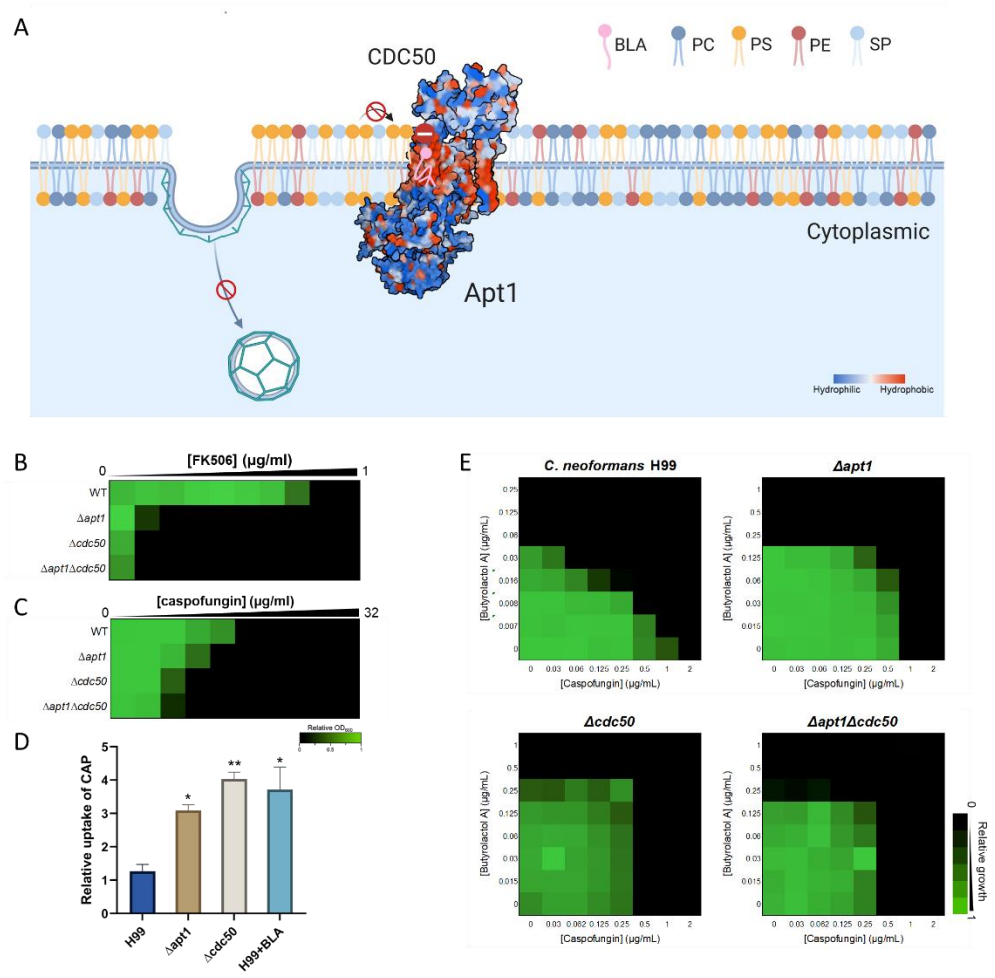

Figure 7. Butyrolactol A (BLA) potentiates the fungicidal activity of caspofungin against Cryptococci by inhibiting the Apt1–Cdc50 complex.

(A) Schematic illustrating the proposed mechanism of action for BLA. The misloading of BLA blocks the entrance of the phospholipid substrate, resulting in impaired membrane asymmetry, which disrupts membrane organization and vesicle budding, ultimately blocking secretory and endocytosis pathways. Color coding is indicated within the figure. (B) Susceptibility of FK506 against *C. neoformans* H99 and flippase-deficient (*cdc50*Δ, *apt1*Δ, and *apt1*Δ *cdc50*Δ). A broth microdilution assay was performed in RPMI 1640 medium, and growth was measured by absorbance at 530 nm after 48 hours at 30 °C. Results are analyzed and depicted as described in Figure 5F. (C) Susceptibility of caspofungin against *C. neoformans* H99 wild type, *apt1*Δ, *cdc50*Δ and *apt1*Δ *cdc50*Δ mutants. Dose-response assays were performed, and data were analyzed as described in Figure 5F. Relative growth is represented quantitatively by color (see bar for scale). (D) Relative caspofungin accumulation in *C. neoformans* H99 wild type, with or without BLA, and in *apt1*Δ and *cdc50*Δ mutants after 15 minutes of treatment. All experiments were performed in biological triplicates, and data are presented as mean ± SD. Significance was

determined using multiple unpaired t-tests, comparing the wild-type without BLA to each group; p-value: *< 0.05, ** < 0.01. (E) The synergistic effect of caspofungin and BLA was assessed against *C. neoformans* H99 wild type, *apt1*Δ, *cdc50*Δ, and *apt1*Δ *cdc50*Δ mutants. Checkerboard assays were performed in SDB medium at 30 °C, and growth was measured by absorbance at 530 nm after 48 hours. Biological duplicates were averaged, and measurements were normalized to no-drug controls and depicted as heatmaps. Relative growth is represented quantitatively by color (see scale bar at the bottom right).